



**HAL**  
open science

# Surface Severe Plastic Deformation for Improved Mechanical/Corrosion Properties and Further Applications in the Bio-Medical and Hydrogen Sectors

Thierry Grosdidier, Marc Novelli, Laurent Weiss

► **To cite this version:**

Thierry Grosdidier, Marc Novelli, Laurent Weiss. Surface Severe Plastic Deformation for Improved Mechanical/Corrosion Properties and Further Applications in the Bio-Medical and Hydrogen Sectors. *Materials Transactions*, 2023, 64 (8), 10.2320/matertrans.MT-MF2022040 . hal-04163204

**HAL Id: hal-04163204**

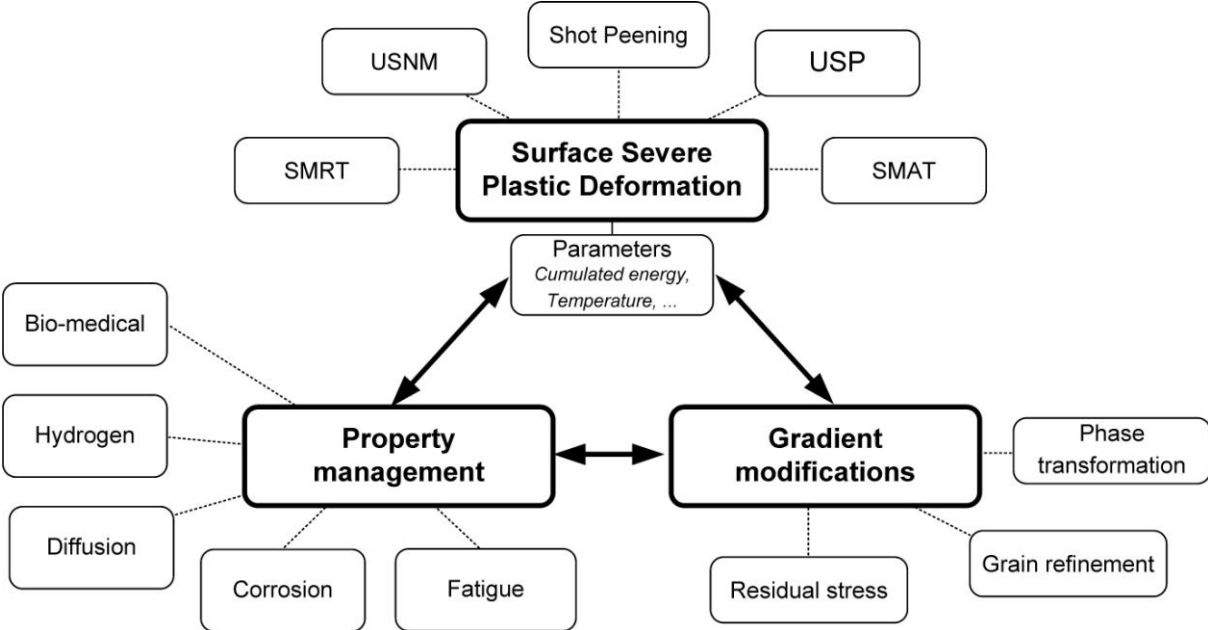
**<https://hal.science/hal-04163204>**

Submitted on 17 Jul 2023

**HAL** is a multi-disciplinary open access archive for the deposit and dissemination of scientific research documents, whether they are published or not. The documents may come from teaching and research institutions in France or abroad, or from public or private research centers.

L'archive ouverte pluridisciplinaire **HAL**, est destinée au dépôt et à la diffusion de documents scientifiques de niveau recherche, publiés ou non, émanant des établissements d'enseignement et de recherche français ou étrangers, des laboratoires publics ou privés.

1 Graphical abstract



2

3

## Surface severe plastic deformation for improved mechanical / corrosion properties and further applications in the bio-medical and hydrogen sectors

Thierry Grosdidier<sup>1,2,\*</sup>, Marc Novelli<sup>1,2</sup>, Laurent Weiss<sup>1,2</sup>

<sup>1</sup> Université de Lorraine, Laboratoire d'Etude des Microstructures et de Mécanique des Matériaux (LEM3 UMR 7239), 7 rue Félix Savart, BP 15082, Metz F-57073, France

<sup>2</sup> Université de Lorraine, Laboratory of Excellence on Design of Alloy Metals for low-mass Structures (DAMAS), Metz F-57045, France

### Abstract

Various techniques enabling surface severe plastic deformation (SSPD) have been developed or optimised over the past years. This manuscript presents a broad overview of recent developments in the field of SSPD and its application that take advantages of having a deformed gradient surface with both (i) higher strength and (ii) an improved "reactivity". First, the principle and technological advantages/disadvantages of several SSPD technologies, involving either guided or non-directional mechanical impacts, are recalled. Then, after a short recall on the nature of the modified surface structure formed under SSPD, the effects of the processing parameters and temperature of deformation on the surface roughness and subsurface microstructure modifications are illustrated with a particular emphasis on the surface mechanical attrition treatment (SMAT) and ultrasonic shot peening (USP) techniques deriving from the traditional pre-strain shot peening. The effect of these surface and sub-surface modifications on the mechanical properties, and in particular the fatigue response, are recalled with a special emphasis on the surface integrity and potential over shot peening. Then, the manuscript concentrates on the effect of the surface enhanced diffusion of chemical species induced by the presence of structural defects to modify the corrosion behaviour and enhance the potential assisted SSPD + thermo-chemically "duplex" treatments. In these cases, in addition to induce grain refinement and dislocations, the importance of controlling some potential surface contamination is stressed. Finally, the manuscript terminates by illustrating some new research studies on potential applications for the challenges in the hydrogen sector for its solid-state storage and the protection of mechanical infrastructures as well as for bio-medical applications with biocompatible Ti-based alloys and biodegradable Mg-based ones.

*Keywords: surface severe plastic deformation (SSPD), shot peening (SP), surface mechanical attrition treatment (SMAT), ultrasonic shot peening (USP), gradient structure, fatigue, corrosion, hydrogen storage, hydrogen protection, bio-medical applications.*

### Corresponding author

[thierry.grosdidier@univ-lorraine.fr](mailto:thierry.grosdidier@univ-lorraine.fr) | Professor at Université de Lorraine, Laboratoire d'Etude des Microstructures et de Mécanique des Matériaux (LEM3 UMR 7239), 7 rue Félix Savart, BP 15082, Metz F-57000, France | +33 3 72 74 78 36

## 43 **1. Introduction**

44 NanoCrystalline (NC) materials (generally associated by metallurgists to materials having an average  
45 grain size lower than 100 nm) and Ultra Fine Grain (UFG) materials (having a sub-micrometric grain  
46 size) have received increasing attention [1]. In terms of mechanical properties, they have an inherent  
47 high strength compared to standard coarse grained (CG) materials together with low temperature  
48 superplasticity or improved creep resistance [2]–[4]. Their functional properties are also appreciated for  
49 potential applications in a wide variety of technological areas such as corrosion resistance, catalysis,  
50 biotechnology, photocatalytic CO<sub>2</sub> conversion, superconductivity, thermoelectric performance,  
51 hydrogen storage, etc [1]–[4]. In this context, processes have been developed to produce - using a  
52 top-down approach in which the microstructure of a bulk material is refined by Severe Plastic  
53 Deformation (SPD) - NC or UFG structures within components [2]–[4]. However, because of the load  
54 required to deform the parts containing a bulk refined microstructure and the associated reduction in  
55 ductility, some of these techniques can be rather difficult to implement in industry.

56

57 As the failure of engineering materials is often initiated from the surface because of local overload,  
58 corrosion, fatigue, and wear, deformation treatments focusing on the modification of the outer part of a  
59 work piece have also been developed. Even if the process of pre-strain Shot Peening (SP) was  
60 considered as rather unpredictable during the early 19th century, continuous research has been  
61 conducted from 1920s onwards on SP that is now introduced into the product design specifications of  
62 numerous industrial components [5]. The use of intense plastic deformation through Surface Severe  
63 Plastic Deformation (SSPD) is more recent to treat some specific zones or critical parts of engineering  
64 materials and, thus, enhance their performances. SSPD can be imparted either (i) directly, by  
65 mechanical shocks [6]–[12] or continuous contact [13], [14] or (ii) indirectly, by using pulsed laser [15],  
66 [16] as well as pulsed ion or electron beam treatments [17]–[19].

67

68 The present contribution will essentially focus on SSPD imparted by mechanical shots using processes  
69 deriving from the traditional pre-strain SP but involving much longer treatment durations and often  
70 higher velocity of the shots. After a short description of some of these techniques (Section 2) a  
71 description of the gradient microstructure thereby generated and the effect of the processing parameters  
72 (impact energy as well as treatment temperature) will be treated in Section 3. Then, after a short recall of  
73 the effect of these hardened gradient surfaces on mechanical properties (Section 4), the interest of  
74 having an improved surface “reactivity” produced by SSPD will be illustrated in Section 5 for different  
75 purposes such as corrosion resistance, "duplex" surface treatments as well as for potential applications  
76 and challenges in the hydrogen sector and population ageing for bio-medical applications.

77

## 78 **2. Shot peening and derived techniques of surface severe plastic deformation techniques.**

79 The following paragraph intends to describe different methods used to introduce properties gradients at  
80 the surface of material with a focus on shot peening and its derivatives. A more exhaustive lists of  
81 mechanical surface treatments can be found in the article of Schulze *et al.* [20].

82 Figure 1 shows a schematic representation of the most common mechanical surface treatments. On top  
83 are presented processes based on directional and guided impacts. Two configurations are shown where  
84 i) the deformation tool is in continuous contact and rolls on the surface to be treated (Figure 1a) or ii)  
85 numerous located impacts are generated by the tool (Figure 1b). The first one consists in applying a  
86 force to a tool in continuous contact with the surface to be deformed and having a spherical tip or a  
87 pressure roller. One of the most common denomination for these processes is deep rolling [21] but can  
88 also be found as Surface Mechanical Rolling Treatment (SMRT) [22]. This type of treatment presents  
89 the advantages to induced deep gradient modifications without a substantial increase in surface  
90 roughness. Concerning the second one, instead of applying a constant load on the surface to be  
91 deformed, localized controlled impacts are used to deform the surface. This can be done with a  
92 conventional hammering device [20] but also, on a smaller scale, by using smaller ultrasonic impacting  
93 tips in the Ultrasonic Surface Nanocrystallization Modification (USNM) process [23]. One limit of such  
94 treatments, weather they are in continuous contact or intended to repeatedly impacting the surface, is  
95 that they are more particularly adapted to revolution parts and plates. A setup where the rolling is  
96 assisted by ultrasonic vibration can also be found [24].

97

98 In order to process part with more complex shapes, other means of surface deformation have been  
99 developed based on directional non-guided impacts. These include treatments based on the projection of  
100 hard particles, the most popular being the shot peening processes [25], [26]. Examples are schematized  
101 in Figures 1c and 1d. They consist of projecting medias having a hardness higher than the part to be  
102 treated and are usually in the shape of spherical particles or cut-wire (cylindrical particles) with a single  
103 size distribution. It has to be noted that mechanical milling apparatus are sometimes used to produced  
104 impacts and referred, for example, as Surface Nanocrystallization and Hardening (SNH) [27]. They will  
105 not be described in this article. Usually, the shots are set in motion either by a centrifugal blast wheel as  
106 in the Rotationally Accelerated Shot Peening (RASP, Figure 1c) or blasted using compressed air as in  
107 the Air Blast Shot Peening (ABSP, Figure 1d). The deformation is imparted by the kinetics energy of the  
108 projected medias. The selection of the medias (shape, size and nature) and the control of their velocities  
109 (by controlling the rotating speed or air pressure) are the main factor influencing the gradient properties  
110 induced to the treated part.

111

112 The most interesting property of the shot peening treatments is the generation of a compressive residual  
113 stress gradient at the surface required to delay crack initiation and propagation during cyclic loadings.  
114 The Conventional Shot Peening (CSP) can also be used to shape thin parts by deformation  
115 accommodation so it is referred as peen forming [28]. The creation of compressive residual stress on the  
116 treated surface and tensile residual stresses on the opposite surface will force the sheet part to bend. It  
117 can also be used to correct the dimension / tolerance of parts during processing. However, one drawback  
118 of the SP treatments is the substantial modification in surface roughness induced after numerous  
119 impacts. As a rough surface can significantly contribute to surface crack initiation via stress  
120 concentrations sites, efforts have been made to associate the beneficial effect of the compressive

121 residual stress state generated by impacts with a reduction of the roughness. One approach consists of a  
122 multi-step SP, also found as re-peening [29]. The principle is to firstly peen the surface with rather high  
123 peening intensity and then re-peen it with smaller medias and/or a lower intensity in order to smooth the  
124 roughness generated at the first step.

125

126 The last category of processes presented in Figure 1 is based on non-directional non-guided impacts. In  
127 this configuration the medias are set in motion in a confined chamber. The shots are then set in motion  
128 either by a translating plate driven by an eccentric (Figure 1e) or by a high frequency resonating  
129 sonotrode (Figure 1f). These techniques are referred as Surface Mechanical Attrition Treatment  
130 (SMAT) or Ultrasonic Shot Peening (USP) [11], [30]. The major difference with the CSP treatments  
131 resides in the fact that the shots have a wide variety of incidence angles when colliding onto the surface.  
132 In this way, the multi-directional impacts bring the advantage of generating more efficiently a thicker  
133 UFG layer at the surface (see Section 3). The amplitude and frequency are the parameters influencing  
134 the initial shot speed (when in contact with the moving / vibrating part). However, the number of shot  
135 and the volume of the chamber are also a determining parameters since they influence the final impact  
136 speed (collision to the surface) due to several interactions dissipating gradually the kinetics energy  
137 through shot/shot or shot/chamber interactions [31]. Finally, the treatment duration will be directly  
138 linked with the total accumulated energy/deformation imparted to the surface. In the case of the  
139 Vibratory Peening (VP, Figure 1g), the whole vibrating chamber is filled with medias in which the part  
140 is completely immersed. This process combines the effects of the CSP by introducing compressive  
141 residual stresses to the surface and the ones of the vibratory finishing by reducing the surface roughness.  
142 It has been documented that the impact velocity component normal to the surface is responsible of the  
143 deformation and the creation of compressive residual stresses whereas the tangential component  
144 generates friction and smoothen the treated surface [32]. This treatment can produce compressive  
145 residual stress gradient comparable to those generated with a CSP treatment [33].

146

147 The SSPD technics based on the projection of shots have a clear advantage when treating parts with  
148 complex shapes like gears, wheels or turbine blade. Due to the plastic deformation capacity of metals  
149 and the resulted deformation gradient (strain hardening, compressive residual stress...), these  
150 techniques are usually applied on metallic materials but can also be used on ceramics [5], [34] or  
151 composites [35]. They can be easily implemented at an industrial scale, can be automatized [36], [37]  
152 and produce a small amount of waste in comparison to thermochemical surface processes. The affected  
153 depth depends on the contribution of all the treatment parameters (shot and material initial hardness,  
154 temperature, duration...) - as will be detailed in section 3 - and the gradient can be produced, both in  
155 terms of microstructure and residual stresses, along several tens to some hundreds of microns depending  
156 on the material and the exact processing parameters.

157 As will be illustrated in the following sections, the SSPD techniques can have some drawbacks and some  
158 limitations that have to be carefully considered. As the peening treatments are based on impacts with the  
159 surface, the surface integrity can be deteriorated when intense conditions are used. This phenomenon is

160 reported as an Over Shot Peening (OSP) [12] and will be highlighted along with potential solution in  
161 Section 4. Additionally, inclusions from the processing media or local contaminations by abrasion of the  
162 treatment chamber are also important factors affecting the local surface reactivity. The presence of  
163 surface contamination is now clearly established and depends on the exact processing material and  
164 conditions [38]. Fe and Cr can be introduced from the stainless steel balls and chamber walls [39], Al  
165 and Zr from the ceramic shots [40], while Ti (+ Al and V) come from the sonotrode when an ultrasonic  
166 device (generally steel or Ti alloy) is used [40], [41]. In particular, the nature of these contaminations  
167 can affect significantly the corrosion behaviour, as will be recalled in Section 5.

168

### 169 **3. The gradient microstructure, how to modify it efficiently**

#### 170 **3.1. Nature of the gradient microstructure**

171 For any application, the metallurgical and microstructural states of the deformed surfaces have to be  
172 tailored - by modifying the processing parameters - in a reproducible manner to form a controlled  
173 gradient microstructure. Taking into account the structure of the grains and their misorientation, the  
174 gradient microstructure generated by any SSPD is generally schematically depicted as the succession of  
175 three (or four if the NC zone is included) different zones: (i) the UFG zone - which also contains the NC  
176 zone present at the extreme top surface - containing randomly oriented grains separated by the high  
177 angle grain boundaries, (ii) the “transition zone” where grains were fragmented under the heavy plastic  
178 deformation and, finally, (iii) the “deformed zone” where the initial grains are simply deformed  
179 [42]–[44]. A schematic representation of these different zones (layers) is given in Figure 2a while,  
180 applied to SMAT, Figure 2b gives an estimate of the different zone thicknesses in a stainless steel  
181 deformed by different magnitude of the processing parameters (see comments in Section 3.2). It must be  
182 recalled however that the transition between these different schematic layers is quite continuous and that  
183 there is no distinct and clear transition between them.

184

185 The grain refinement process depends on the deformation mechanisms (twinning, dislocation  
186 activities...) involved under the SSPD loading coupled with potential dynamic recrystallisation /  
187 recovery processes. In the case of steels for example, the relevant material property commonly used to  
188 determine the plastic deformation accommodation mechanisms is the stacking fault energy (SFE).  
189 When the SFE is high, dislocation activity and rearrangement are formed during deformation leading to  
190 dense dislocation walls and tangles to refine the material microstructure, as observed in pure Fe ( $\sim 200$   
191  $\text{mJ.m}^{-2}$ ) [45]. Medium SFE promotes twinning to accommodate the deformation – as observed in  
192 Fe–Mn–C alloys [46] (12 to 35  $\text{mJ.m}^{-2}$ ) - and the structural refinement is driven by twin/twin  
193 interactions or twin fragmentation. When the SFE becomes low, a deformation induced martensitic  
194 transformation can be triggered like in metastable austenitic stainless steels [47]–[49] ( $< 20 \text{ mJ.m}^{-2}$ ).  
195 While for face-centred cubic (FCC) and body-centred cubic (BCC) metals, the grain subdivision to  
196 accumulate strains takes place by the formation of dislocation cells and dense dislocation walls at high  
197 SFE, deformation induced twinning is always prevalent for hexagonal close packed (HCP) metals  
198 because of the limited number of slip systems, at least in the early stages of deformation [50], [51].

199

200 In addition to the modification of the grain size through the depth of the samples, the gradient  
201 microstructure can be in some cases the superimposition of different gradients : one in terms of grain  
202 size, the other one in terms of phase distribution for example [49]. A detailed analysis of the effect of  
203 various processing parameters - including the use of cryogenic temperature for processing - on the 304L  
204 steel revealed that, in such TRansformation Induced Plasticity (TRIP) steels, the maximum amount of  
205 martensite was never found in the vicinity of the extreme surface, where the finest grains were present,  
206 but at 50 to 100  $\mu\text{m}$  below the surface depending on the processing conditions. This aspect is important  
207 to interpret correctly the hardening in SSPD materials in which a phase transformation can take place.  
208 The modification of the exact nature and the depth of the gradient structure can be done by changing the  
209 “conventional” processing parameters, which will modify the energy imparted by the impacting media  
210 (pin, ball, harmer...), and/or the processing temperature.

211

### 212 **3. 2. Effect of the impact energy through “conventional” processing parameters**

213 The energy imparted to the surface depends on the impact density and the shot velocities. They are the  
214 result of a combination of various processing parameters such as the shot characteristics (quantity,  
215 diameter and nature), the vibrating amplitude that set the shots in motion and the duration of the  
216 treatment. Several research works have investigated the effects of the processing parameters. Chen *et al.*  
217 [52] used two sets of SMAT processing parameters (vibrating frequencies, nature and diameter of the  
218 balls) to treat the 304 stainless steel under low (0.5 m.s<sup>-1</sup>) and high (10 m.s<sup>-1</sup>) speeds of the shots. For  
219 similar surface hardness, different sub-surface hardness gradients were obtained resulting in different  
220 mechanical behaviour of thin (1 mm) plates treated on both sides. Several pioneer results [52]–[54] have  
221 shown that increasing the energy imparted to the surface allows to increase the material hardness deeper  
222 in the material.

223 However, the control of this evolution, as well as the separate effect of the processing parameters,  
224 remains generally quite qualitative. In order to characterize quantitatively the thickness of the different  
225 layer of the graded structure, Samih *et al.* [42] have established an automated procedure - based on an  
226 analysis of Geometrically Necessary Dislocations (GNDs) coupled with indexing and size criteria -  
227 obtained from various Electron BackScattered Diffraction (EBSD) maps carried out at different  
228 magnifications. As illustrated in Figure 2b, under their tested processing conditions - varying the  
229 amplitude of vibration (in  $\mu\text{m}$ ) and treatment duration (in min) - these authors have established that the  
230 UFG and transition zones were more significantly modified than the overall affected thickness for a  
231 316L stainless steel. Also, trying to increase the treated depth by using an increase of the intensity of the  
232 peening parameters has a limit because the top surface will lose its integrity and result in crack initiation  
233 under too severe loading. As it will be illustrated hereafter, an effective way to modify the affected depth  
234 and the evolution of the sub-surface hardness (and residual stress gradient) is to modify the processing  
235 temperature.

236

### 237 **3. 3. Effect of the shot peening temperature**

238 One of the important processing parameters that has received so far little attention is the temperature at  
239 which the shot peening is carried out. Processing by SPD of bulk material at Cryogenic Temperature  
240 (CT) prevent dynamic recovery and stimulate mechanical twinning in order to, in both cases, enhance  
241 the grain refinement. To reduce further the size of the surface microstructure, cryogenic surface  
242 treatments have also been developed such as cryogenic burnishing [55], [56], cryogenic laser shot  
243 peening [57], cryogenic impact [58], [59], as well as the SMAT/USP processes applied at low  
244 temperature [49], [60]–[65]. It is also interesting to change the peening temperature in order to modify  
245 the deformation modes in alloys for which twinning or martensitic transformation can compete with  
246 conventional slip systems to accommodate plastic deformation. In a comparative analysis of the SMAT  
247 behaviour of two austenitic stainless steels having very different stabilities of their austenitic phases,  
248 Novelli *et al.* [60] have shown that, in addition to surface hardening, the most interesting result was a  
249 significant increase in the subsurface hardness for the steel in which the strain induced martensitic  
250 transformation deeper in the subsurface. This is illustrated in Figure 3. At CT, for the 304L steel ( $Md_{30} =$   
251  $21^{\circ}\text{C}$ ), the martensitic transformation is promoted for lower stress/strain and, thus, deeper towards the  
252 depth of the sample (single arrow). Comparatively, the 310S steel, which is extremely stable against the  
253 martensitic transformation ( $Md_{30} = -169^{\circ}\text{C}$ ), is harder to deform plastically and its subsurface hardness  
254 reduces (double arrow). Thus, peening at CT can be justified for this kind of TRIP steels if additional  
255 subsurface hardenings are targeted.

256

257 As just stated, because the strength of the material increases at CT, in the absence of martensitic  
258 transformation, it becomes more difficult to impart plastic deformation at the depth of the treated  
259 sample. In this case, to improve the sub-surface hardness, processing must be done at higher  
260 temperature. Thereby, as the yield limit of a metal decreases when heated, higher subsurface hardening  
261 and larger maximum compressive residual stresses can be achieved. This is illustrated for hardness in  
262 Figure 4 taken from the work of Wang *et al.* [66]. The higher compressive residual stress gradients also  
263 have an improved stability, as observed by Wick *et al.* [67]. Therefore, as proved by results on steels  
264 [66], [67] and Mg alloys [68], increasing slightly the peening temperature can be a good idea to improve  
265 the fatigue life or fatigue strength. The increase in peening temperature generally generates higher  
266 subsurface hardening and larger maximum compressive residual stresses. Therefore, for an optimum  
267 Almen intensity, the surface of the warm shot peened specimen is more plastically deformed but less  
268 "damaged" due to the increase in plastic deformation ability [68]. Also, the dislocation structure is likely  
269 to be modified towards a higher stability [67].

270

271 It is also important to mention that, additionally, in-situ diffusion phenomenon can take place during  
272 warm treatments. Ye *et al.* [69] have observed the formation of more nanoprecipitates in an AA6061  
273 aluminum alloy and Wick *et al.* [70] the precipitation of fine carbides in the microstructure of an AISI  
274 4140 deformed by warm peening. These fine solutes contribute to pin and impede the movement of  
275 dislocations, thus raising the mechanical resistance. Dynamic recrystallization is also a mechanism to  
276 consider during warm surface treatment. Due to the energy stored by plastic deformation, microstructure

277 restoration and /or recrystallization can take place, as observed by Pan *et al.* [71] and Kikuchi *et al.* [72].

278

279 These kinds of treatment are usually referred as heat-assisted surface mechanical treatment [73].

280 Different ways can be found in the literature to heat the sample like a pre-heat in furnace [74], heating

281 plate with electric resistances [75], the Joule's effect [76] or infrared radiation [77]. Only two articles

282 have reported on the effect of heat-assisted SMAT. Wei *et al.* [78] used a pre-strain warm SMAT / USP

283 to deform the surface of a NiTi alloy. They managed to increase the bending fatigue by 13 times using a

284 combination of a finer surface microstructure, a deeper hardness gradient and higher compressive

285 residual stresses. Comparatively, Kong *et al.* [79] applied a temperature-assisted USP on a two phases

286 Mg-Li alloy. They reached a deeper hardening under warm condition but this was associated with a

287 decrease in hardness. The smallest surface grain size was achieved with a peening of 100 s at 100°C.

288

289 As pointed out in several contributions under warm conditions [66]–[68] or CT [49], the peening

290 temperature has a strong effect on the surface roughness evolutions. Because the material becomes

291 softer, the surface roughness increases when the peening temperature is raised. For ultrasonic shot

292 peening, the amplitude of the sonotrode, that is inducing the kinetic energy to the flying shots, is also a

293 factor affecting strongly the surface roughness. Thus, for a given type of shots (size and weight), the

294 highest roughness is generally obtained for the highest amplitudes of the sonotrode and/ or higher

295 peening temperature. On the other hand, it is possible to lower the roughness by using a “moderate”

296 sonotrode amplitude, increasing the treatment time and, more significantly, by lowering the peening

297 temperature. Adapted from [49], Figure 5 illustrates, for two types of steels, the direct correlation

298 between the surface roughness and top surface hardness for different sets of processing parameters.

299 Thus, the use of temperature is an additional parameter during ultrasonic SMAT that allows to tailor the

300 surface properties towards tribological applications by controlling the surface hardness and roughness

301 rather independently.

302

#### 303 **4. Gradient structures and improved mechanical properties.**

304 The overall material properties can be significantly enhanced through the formation of

305 gradient-structures with refined surface microstructures [80]. Considering steels for example, besides a

306 conventional use to harden the surface and improve wear [81], [82], tensile properties of the 316L [83]

307 and the 304 [53], [84] stainless steels were also improved while multi-layered laminate composites were

308 created by SMAT and subsequent roll bounding [85]. To this respect, in addition to the contributions of

309 the finer grains in the surface layer and the high dislocation density produced by SMAT, the presence of

310 residual stresses has also been demonstrated to contribute substantially to the improved tensile

311 properties [86]. While the compressive residual stress (CRS) into the surface layer directly contribute to

312 the enhancement in yield strength, the tensile / compressive layers contribute also by developing strong

313 hetero-deformation induced (HDI) hardening. The hetero-zones deform inhomogeneously, generating

314 back stresses in the soft zone and forward stresses which, together, produce this HDI strengthening that

315 increases yield strength and enhance strain hardening, thus and helping to retaining ductility [87], [88].

316 The HDI strengthening, which comes from the mutual constraint of the hard and soft zones, is active in  
317 many types of heterostructured materials containing for example laminate, gradient or core-shell  
318 structures and possessing superior combinations of strength and ductility [88].

319

320 The major mechanical response targeted through SSPD techniques derived from SP remains the  
321 optimisation of the fatigue properties. Several review papers dealing with the fatigue behaviour of  
322 metals subjected to different types of SSPD treatments have been published recently [89], [90]. Factors  
323 affecting the fatigue life of a component can be roughly divided into two main categories. First, the  
324 surface roughness or the presence of stress raisers, influence essentially the initiation stage of crack  
325 growth [91]. Second, the presence of residual stresses and structural defects which affects the crack  
326 propagation mechanics [86], [92]–[94]. The association of a superficial refined microstructure and a  
327 high compressive residual stress gradients produced by SSPD, and in particular SMAT / USP, has been  
328 shown to delay the crack initiation and impede its propagation on a wide range of materials such as Fe  
329 [95], Ti [96] or Mg [97] -based alloys. If the use of mechanical surface treatment allows to push the  
330 initiation site under the peened surface and that deeper compressive residual stresses are known to  
331 improved fatigue properties, an excess of peening energy can also affect the surface integrity which can  
332 impede the fatigue resistance of the components [96], [98], [99]. Concerning crack initiation, for  
333 precipitation hardenable Al-based alloys, the effect of SMAT before or after precipitation aging has  
334 been investigated by Maurel *et al.* [99]. It was shown that a high notch sensitivity (7075) should not be  
335 processed by SMAT, as the generated low surface integrity is always detrimental to fatigue  
336 performances. On the contrary, for a less notch sensitive alloy (2024), SMAT prior to aging formed  
337 smaller and denser precipitates - resulting in a high-hardened depth - and microstructures more resistant  
338 to residual stress relaxation than after conventional shot peening. SMAT after aging resulted in a  
339 significant improvement of fatigue performance with only subsurface crack nucleation sites for the same  
340 2024 alloy [99]. Concerning the relaxation of the compressive residual stresses, Dureau *et al.* [100] have  
341 compared the fatigue performance of a SMATed austenitic stainless under two fatigue load ratios: fully  
342 reversed Tension-Compression (TC)  $R_{TC} = -1$  and Tension-Tension (TT)  $R_{TT} = +0.1$  After identical  
343 SMAT processing conditions, the fatigue limit was enhanced by +17% for  $R_{TC}$  while it was reduced by  
344 -7% for  $R_{TT}$ . The residual stress measurements have revealed that, while the stress gradient was simply  
345 smoothed after the  $R_{TC}$  fatigue loading, it was completely reverted for the  $R_{TT}$  one. The fatigue crack  
346 initiation sites and propagation were significantly modified between the  $R_{TC}$  and  $R_{TT}$  loading conditions  
347 [100]. Finally, considering the phenomenon of Over Shot Peening (OSP), a novel shot peening  
348 treatment called gradient Severe Shot Peening (SSP) has been introduced recently by Maleki *et al.* [12]  
349 to mitigate the problem of losing surface integrity and weakening the fatigue properties. Instead of using  
350 constant projection pressure of the shots, as during conventional SP, this treatment implements  
351 gradually increasing or decreasing pressures. Significant fatigue life improvements were obtained for  
352 SSP treated specimens because SSP avoided the detrimental effects of over-peening while maintaining  
353 the beneficial effects of surface nano-crystallization, surface hardening and compressive residual  
354 stresses [12].

355

**356 5. Gradient microstructure and improved surface reactivity**

357 The high fraction of structural defects (i.e. High Angle Grain Boundaries (HAGB), Low Angle Grain  
358 Boundaries (LAGB), dislocations...) induced by SSPD can lead to a significant increase in stored energy  
359 which, inevitably, increases the material reactivity and the diffusion of chemical species. In addition to  
360 modify the corrosion or oxidation properties, these refined surface structures have been proved to  
361 activate the kinetics of chemical reactions and several “duplex” mechanically-assisted thermochemical  
362 treatments have been developed or improved. In addition, some potential applications of SSPD are  
363 raising in the hydrogen sector and for bio-medical applications.

364

**365 5. 1. Corrosion resistance**

366 Several initial studies on the effect of SPD on the corrosion response have revealed either beneficial or  
367 deleterious effects (see for example [101]) indicating also that the literature was insufficient to find  
368 general trends example [102]. There is nowadays a significant amount of research concerning the  
369 corrosion behaviour of metals treated by shot peening (or its derivative SMAT and USP types of  
370 technology) indicating that other factors than the grain size and/or the amount of structural defects must  
371 be taken into account [101]. Obviously, the higher reactivity may not be suitable or lead to a dual  
372 behaviour depending on the material environment. Indeed, improvements or deleterious effects can be  
373 obtained for the same material depending on the location on the  $E_n$ -pH Pourbaix diagram. SPD improves  
374 the corrosion resistance in a passive environment whereas it increases the dissolution rate in a  
375 non-passive environment [103]. In the case of stainless steels, for example, a decrease in corrosion  
376 resistance is reported in depassivating electrolytes while the higher reactivity of the SMATed surface  
377 helps to create faster a passivating (i.e. protective) film in many aqueous environments [104], [105]. The  
378 corrosion resistance can also depend on the processing route used to generate the structure [106].  
379 Indeed, these processing routes generally affect other parameters than the grain size such as the  
380 chemical homogeneity, size and distribution of inclusions, dislocation densities or solid solubility;  
381 parameters which are equally important for corrosion properties. Strain induced precipitate coarsening  
382 was observed in a Ti-Nb-Sn orthopedic alloy after SMAT, which increased marginally its corrosion rate  
383 [107]. Comparatively, on a 301 stainless steel, SMAT improves the diffusion of Cr on the surface to  
384 form a stronger and better passivation layer [108].

385

386 As mentioned in Section 2, contamination can be introduced by the peening medias that are also able to  
387 transfer chemical elements from both chamber and sonotrode to the sample surface, modifying thereby  
388 locally the chemical composition of the treated surface and so affecting the corrosion behaviour. Wen *et*  
389 *al.* [109] have demonstrated that the corrosion resistance of a 2024 Al alloy was directly affected by the  
390 nature of the shot peening media. Indeed, while the NC layer fabricated by SMAT with ceramic balls  
391 improved the corrosion resistance because of the formation of a dense passive film, the Fe containing  
392 layer induced by SMAT with the steel shots led to galvanic corrosion reaction between Fe and Al [109].  
393 In accordance with this result, a recent analysis of the corrosion in two aluminium alloys (AA 2024 and

394 AA 7150) has shown the dual effect of such treatment: the dissolution of the nano-sized strengthening  
395 precipitates in the Al matrix and grain refinement generated under the USP treatment have improved the  
396 intergranular corrosion resistance while the overall corrosion rate was increased by the Fe  
397 contamination [110]. To counterbalance, or at least mitigate, the potential effect of the surface  
398 contamination, Murdoch *et al.* [111] have introduced a pre-processing step (pre-coating of the shot  
399 media and chamber) to reduce the resulting impact on corrosion properties.

400

## 401 **5. 2. Use of increased surface reactivity for "duplex" treatments**

402 SSPD processes such as SMAT and USP, thanks to the high quantity of structural defects generated at  
403 the surface and associated enhancement in diffusion, several industrial thermochemical treatments can  
404 be optimized. These mechanically-assisted thermochemical “duplex” treatments are for example  
405 nitriding [112], pack boronizing [113], aluminizing [114], chromizing [115] as well as plasma  
406 electrolytic oxidation [116].

407 Among these “duplex” treatments, nitriding has been the most widely investigated one. Indeed, for  
408 industrial applications, nitriding can benefit in different ways from the presence of these NC or UFG  
409 surface and gradient structure produced at the deformation stage. First, the enhanced atomic diffusion  
410 and enhanced chemical reaction kinetics can be used either (i) to produce thicker layers or (ii) to lower  
411 the nitriding temperatures [112], [117], [118]. This latter option is very interesting for austenitic  
412 stainless steels. Indeed, carrying the nitriding treatment at temperature as low as 300°C is of primary  
413 importance for the quality of the corrosion properties in austenitic stainless steels because it keeps a  
414 single-phase structure of expanded austenite and avoids the precipitation of Cr-rich nitrides. Second, the  
415 duplex SMAT + nitriding treatment also has the advantage to produce a much harder surface nitrided  
416 layer that forms on a sub-surface hardened substrate [11]. The top surface is hardened by a combination  
417 of both plastic hardening due to the severe deformation and solute hardening due to the presence of the  
418 N-enriched austenite while the subsurface hardening induced by the SMAT is maintained after nitriding  
419 [11].

420 To avoid the contamination produced by SMAT which is acting as a barrier to the nitrogen flux and  
421 leads to the formation of reduced or discontinuous nitriding layers [119], chemical etching [120] or  
422 mechanical polishing [40], [121] must sometimes be used as an intermediary stage during such duplex  
423 treatment in order to reduce the surface contamination and, thereby, improve further the quality and  
424 thickness of the nitrided layers.

425

## 426 **5. 3. Use of SSPD for the hydrogen sector.**

427 To make hydrogen a significant contributor to clean energy transitions, it needs to be adopted in sectors  
428 where it is almost completely absent, such as transport, buildings and power generation. However, clean  
429 widespread use of hydrogen in global energy transitions faces several challenges. In addition to produce  
430 “green” hydrogen, two key issues are also its storage under safe conditions and its transportation.

431

### 432 **5. 3. 1. Hydrogen solid-state storage**

433 A considerable amount of research has been devoted to develop advanced H-storage media in solid-state  
434 materials by forming metal hydrides [122]. Magnesium and its alloys have attracted significant interest  
435 in the field of hydrogen storage owing to their high hydrogen-storage capacity, low-cost and abundance  
436 in Earth's crust. However, the high thermodynamic stability of Mg-H bond as well as sluggish sorption  
437 kinetics limit their practical applications [123]. Microstructure refinement using various processes such  
438 as High Energy Ball Milling (HEBM) of powders or severe plastic deformation have been used to lower  
439 the hydrogenation/dehydrogenation temperature and increase the reaction rates in Mg-based materials  
440 [124]. Despite significant output, the HEBM process is prohibitive because it is time- and  
441 energy-consuming as well as because handling pyrophoric powders raises severely safety concerns.  
442 Other metallic systems based on Ti-V-Cr or FeTi have a lower storage capacity but authorises the  
443 reversible transformation near room temperature. However, while materials based on these systems can  
444 thermodynamically store hydrogen at RT, their hydrogenation requires a first "activation" process at  
445 high temperature and/or under high pressure to react with hydrogen during the first hydrogenation cycle  
446 [125], [126]. Edalati *et al.* reported that SPD applied of TiFe by High Pressure Torsion (HPT) can  
447 activate the material to reversibly absorb and desorb hydrogen at RT without any conventional  
448 activation heat-treatment; and this even after 400-day storage in air [127]. It was suggested that the main  
449 mechanism for the HPT-induced activation was the formation of large fraction of grain boundaries  
450 acting as pathways for hydrogen. Comparatively, the room-temperature hydrogenation capability of  
451 alloys based Ti-V-Cr was possible but their reversibility was degraded by the presence of structural  
452 defects [128], [129]. Avoiding the introduction of structural defects and fine gains within the overall  
453 sample as is the case for HPT, a gradient microstructure produced by SMAT was proved to be an  
454 effective way to activate the material so that it could subsequently reversibly absorb and desorb  
455 hydrogen at RT [129], [130]. As illustrated in Figure 6, the gradient structure created by SMAT has its  
456 own advantages. First, the nanostructure and cracks present at the surface of the SMATed sample could  
457 act as a pathway for hydrogen transport through the oxide layer and activate the material for H-storage.  
458 Second, the H-atoms could be stored in the defect-free subsurface were more reversibility is expected.  
459 Thus, processes inducing surface gradients can be regarded as having a high potential for elaborating  
460 industrially H-storage materials [130].

461

### 462 **5. 3. 2. Hydrogen protection**

463 When hydrogen diffuses into a metal, it can decrease its mechanical resistance by a localization of the  
464 hydrogen concentration at microstructural defects. This phenomenon is known as Hydrogen  
465 Embrittlement (HE) and several HE theories have been documented to explain this behaviour like  
466 Hydrogen-Induced Phase Transformation (HIPT), Hydrogen-Enhanced DEcohesion (HEDE),  
467 Hydrogen-Enhanced Localized Plasticity mechanism (HELP) or Hydrogen-Enhanced Strain-Induced  
468 Vacancies (HESIV) [131]. As the hydrogen is absorbed and diffuse within a material from the surface,  
469 surface functionalization has been tested in order to prevent or reduce phenomenon liked HE. It can take  
470 the form of surface chemistry modifications like coatings but also mechanical surface treatments [132].  
471 Most of the articles about HE reduction using mechanical surface treatment deal with the use of

472 conventional SP applied essentially on steels. An *et al.* [133] reported good tensile and fatigue properties  
473 after hydrogen charging on a shot peened X80 steel. They suggested that the combined effect of grain  
474 refinement, the high amount of dislocation density and compressive residual stresses decrease the  
475 hydrogen diffusion. More precisely, they proposed that the high density of defects associated to the  
476 accumulation of hydrogen in the shot peened layer (Figures 7a and 7b) is responsible for creating a  
477 mismatch between the treated surface and the non-deformed core, leading to the formation of  
478 sub-surface cracks (Figure 7c) which will then propagate towards the surface (Figure 7d). Makoto *et al.*  
479 [134] also reported that the HE resistance was improved whether the hydrogen charging was carried out  
480 by cathodic charging or by cyclic corrosion tests. They also reported the beneficial effect of compressive  
481 residual stress to reduce hydrogen absorption and thus HE. Wang *et al.* [135] have studied the effect of  
482 SP coverage and intensity on the HE of a hypo-eutectoid steel. The hydrogen diffusivity was decreased  
483 for all peening coverage in three steps. In the CSP regime ( $< 400\%$ ), the hydrogen diffusivity rapidly  
484 decreases by an increase of the hydrogen trapping sites. Then followed a plateau regime in the SSP  
485 range (1000 to 7000 %) due to a limitation of dislocation generation to the benefit of subgrain structure  
486 formation. Finally, the hydrogen diffusivity decreased again when the sample was OSP ( $>12000\%$ ) by  
487 the formation of a fully refined microstructure, further increasing the probability of the hydrogen to be  
488 trapped. The authors suggested that increasing the number of hydrogens trapping site by plastic  
489 deformation is more critical than the presence of compressive residual stress in order to reduce hydrogen  
490 diffusivity and HE in this hypo-eutectoid steel.

491  
492 A more limited amount of work of research has been devoted so far to the use of the less conventional  
493 SSPD techniques. Kim *et al.* [136] used an USNM treatment at RT and elevated temperature ( $300^{\circ}\text{C}$ ) on  
494 a high-Mn steel. Both samples treated by USNM showed less hydrogen content than the untreated  
495 sample due to the presence of compressive residual stress gradients. The creation of  $\epsilon$ -martensite at RT  
496 was the main reason of the mechanical property degradation after hydrogen charging, even compared to  
497 the initial sample. As the strain-induced martensitic transformation was suppressed at higher  
498 temperature of deformation, the sample treated at  $300^{\circ}\text{C}$  showed the lowest decrease in mechanical  
499 properties. Thus, tailoring the deformed microstructure by controlling the phase in presence can increase  
500 the HE resistance as well as the presence of refined grains and compressive residual stress. Safyari *et al.*  
501 [137] processed a 7075-T6 aluminium alloy by USP. They reported that the production of a fine-grained  
502 surface layer allows to increase the HE resistance of the material. Production of smaller grains increases  
503 the grain boundaries surface fraction which then decreases the hydrogen trapping sites per unit length of  
504 grain boundary.

505 More recently, to achieve high yield strength and high ductility in the presence of hydrogen,  
506 Mohammadi *et al.* [138] used low and mild intensity controlled SMAT conditions to generate gradient  
507 structures containing different amount of surface nanotwins in a CrMnFeCoNi high-entropy alloy. They  
508 compared the samples behaviour with its as -received coarse and nanostructured counterparts produced  
509 by high-temperature homogenization and HPT, respectively. In the presence of hydrogen, gradient  
510 samples showed a good combination of high yield stress of 500-700 MPa, which was 2-3 times higher

511 than the yield stress of coarse-grained material, coupled with a high level of plasticity (15-33%). This  
512 study introduced gradient-structured high-entropy alloys as new high-strength materials with high  
513 resistance to HE, particularly when the hydrogen was kept under a critical level to prevent the HELP  
514 mechanisms.

515

#### 516 **5. 4. Use of SSPD for bio-medical applications.**

517 A considerable amount of research has been devoted to the biocompatibility of the SSPD treated  
518 materials. When a prosthesis is placed in a body, the cells react with the surface of the prosthesis  
519 according to its chemical and mechanical properties. Thus, over the past three years, several studies  
520 have characterised the effects of SSPD on cell viability. Two major families of base-metal alloys are  
521 essentially investigated. The first family of alloys for the manufacture of prostheses is titanium because  
522 it is perfect biocompatible and, for the  $\beta$ -Ti alloys, because their Young's modulus (30-60 GPa) are  
523 rather close to bone ones (15-30 GPa) [139]. The second family is magnesium alloys, again because of  
524 the good compatibility of Mg but also because more and more medical studies have focused on  
525 resorbable alloys. The advantage of degradable implants is that they provide mechanical support to the  
526 fractured bone for a short time, while the tissue repairs and remodels. Some recent studies focusing on  
527 the effect of plastic deformation of the surface on biocompatibility are reviewed hereafter for these two  
528 families of alloys.

529

##### 530 **5. 4. 1. Titanium alloys**

531 Agrawal *et al.* have performed short time USP treatments on pure titanium and showed that both the cell  
532 viability and the surface corrosion resistance were significantly improved [140]. The beneficial effect of  
533 USP on cell proliferation was attributed to the nanocrystallisation of the surface coupled with the  
534 increase in positive potential at the treated surface. The improvement in corrosion resistance was due to  
535 the preferential formation of TiO<sub>2</sub> that tended to grow from the high density of grain boundaries. It  
536 should also be noted that performing a vacuum stress relief treatment after USP further improved the  
537 cell viability. The effect of SMAT on pure titanium has also been studied by Luo *et al.* [141]. The in  
538 vitro study on MG63 cells showed that SMAT promoted the adhesion effect and inhibited cell apoptosis.  
539 The authors explain this by an improved mineralisation capacity, improved protein adsorption capacity  
540 and hydrophilicity due to the nanostructuring. In order to clarify which is the predominant parameter  
541 acting on biocompatibility between chemistry, roughness and nanostructuring, Weiss *et al.* performed  
542 SMAT on TiMo and TiNb chemically functionally graded materials (FGM). The overall range of  
543 composition for the FGM span from 100% Ti to 100% Mo (or Nb) [142] and several interesting result  
544 were obtained. Firstly, from a practical experimental point of view, this study has demonstrated that the  
545 use of FGMs allows the study of the effect of severe plastic deformation on several materials in one go  
546 (saving on the number of samples) while ensuring that all the biological tests are performed under the  
547 same conditions. This is illustrated in Figure 8 that compares the effect of three surface conditions  
548 (polishing, SMAT and SMAT+polishing), varying by their roughness and degree of deformation, on  
549 cells adhesion and proliferation. Figure 8 indicates that, from a biocompatibility point of view, the

550 increase in roughness induced by SMAT improve cell adhesion (human mesenchymal stem cells) but do  
551 not alter the proliferative capacity of the cells. Clearly, the results show that the refinement of the  
552 microstructure and the presence of structural defects induced by the surface severe plastic deformation  
553 have an effect on the distribution of cells during the early stages of proliferation. However, in the long  
554 term, it is the alloy chemistry that remains the most important factor in ensuring cell proliferation; with  
555 here niobium being a better alloying element than molybdenum for this purpose [142].

556

557 When applied on  $\beta$ -Ti alloys, SMAT can generate unfamiliar deformation mechanisms such as  
558 kink-bands [143]. A limited surface hardening was observed for an orthopedic Ti-Nb-Sn alloys after  
559 SMAT but SMAT enhanced the cell proliferation rate and, more importantly, the osteogenic  
560 differentiation of stem cells [107]. SMAT treatment followed by calcium ion implantation has been  
561 tested on the Ti-25Nb-3Mo-2Sn-3Zr  $\beta$ -Ti alloy by Huang *et al.* [144]. The SMATed samples showed  
562 improved hydrophilicity compared to the untreated samples. Subsequent Ca ion implantation further  
563 improved wettability. In vitro cell experiments indicated that the SMAT samples promoted cell  
564 adhesion, cell proliferation, osteogenic differentiation, collagen secretion and extracellular matrix  
565 mineralization of Mesenchymal Stem Cells (MSC). The addition of Ca further enhanced MSC adhesion  
566 and osteogenic functions. Thus, following the strategy implemented for more technical issues (see  
567 Section 5.2), this kind of duplex treatment opens up a very interesting avenue of research.

568

569 Laser Shot Peening (LSP) also improved biocompatibility as shown in the study by Vishnu *et al.* on  
570 Ti22Nb alloy [145]. The laser-peened surfaces showed increased cell spreading and anchorage,  
571 attributed to the presence of micro-topography and associated nanoscale features to enhance cell-surface  
572 interactions. Similar features were observed by Zhang *et al.* on NiTi [146]. In addition to an increase in  
573 scratch resistance, electrochemical tests showed an increase in corrosion resistance. Immersion tests in  
574 simulated body fluid indicated that the initial release of Ni ions was inhibited by LSP, especially during  
575 the first week. In addition, LSP improved calcium deposition. The in-vitro study of adipose-derived  
576 stem cells indicated that the Live/Dead ratio, adhesion and propagation were improved by LSP. This  
577 process also allowed Shen *et al.* to improve the wettability of the Ti-6Al-7Nb orthopaedic alloy [147].  
578 Yang *et al.* to increase the resistance of the Ti-3Cu alloy to Staphylococcus aureus bacteria [148] as  
579 shown in Figure 9. This figure illustrates that the antibacterial efficiency increases from 70.7% on an  
580 untreated sample to 98.2% on a sample treated by LSP.

581

#### 582 **5. 4. 2. Magnesium alloys**

583 Vasu *et al.* showed that a Friction Stir Process (FSP) treatment results in the formation of a  
584 nanostructured layer in the ZE41 alloy without changing the corrosion resistance properties [149]. The  
585 prosthesis would therefore have enhanced surface mechanical properties without losing its  
586 biocompatibility. The same process was used by Badisha *et al.* to alloy the surface of a Mg sample with  
587 Zn powder [150]. They manage to obtain a refined surface structure having a lower corrosion rate than  
588 the pure Mg in a simulated body fluid.

589 Manivasagam *et al.* studied the surface of a WE43 alloy deformed by SMAT [151]. They found an  
590 increase in hardness, roughness, surface oxide layer and hydrophilicity, as well as a 90% increase in  
591 corrosion resistance. Human foetal osteoblast (hFOB) cells showed higher biocompatibility on  
592 SMAT-treated substrates, with the bone matrix depositing significantly more  $\text{Ca}^{2+}$ . In addition, a  
593 significant reduction in MRSA (methicillin-resistant *Staphylococcus aureus*) adhesion was observed on  
594 SMAT-treated substrates compared to untreated substrates. The beneficial effect on corrosion remains  
595 debatable as, at the same time, Singh *et al.* measured a lower corrosion resistance on AZ91D alloy after  
596 SMAT [152].

597

## 598 6. Conclusions

599 A broad overview is given here on different aspects related to applications of surface  
600 treatments involving severe plastic deformation with a more specific focus on recent research derived  
601 from shot peening such as the SMAT or USP for example. Considering the structure of the grains and  
602 their misorientation, any SSPD treatment generates a gradient of microstructure with different  
603 transitions ranging from surface NC or UFG highly misoriented grains to large deformed grains towards  
604 the core of the material. Due to the plastic deformation capacity of metals and the resulted deformation  
605 gradient (strain hardening, compressive residual stress...), these techniques are usually applied on  
606 metallic materials but can also be used on ceramics or composites.

607 The SSPD techniques are rather easy to implement in industry and produce a small amount of  
608 waste in comparison with conventional surface thermochemical modification techniques. The short  
609 presentation of the principle of some of these SSPD techniques (Section 2) highlights the interest of  
610 having multidirectional impacts of the shots in a confined chamber, instead of directional ones, in  
611 improving the grain refinement process. As underline in section 3, the grain refinement process depends  
612 on the deformation mechanisms (twining, dislocation activities...) activated on loading, which are  
613 directly related to the crystallographic nature of the impacted material and its stacking fault energy,  
614 coupled with potential dynamic recrystallisation / recovery processes. The control of the peening  
615 parameters and the processing temperature are important parameters to tailor the surface roughness and  
616 the sub-surface properties of the treated parts while avoiding over peening.

617 The affected depth depends on the contribution of all the treatment parameters (shot and  
618 material initial hardness, temperature, duration...) and the gradient can be produced, both in terms of  
619 microstructure and residual stresses, along several tens to some hundreds of microns depending on the  
620 material and the exact processing parameters. In addition to the contributions of the finer grains in the  
621 surface layer and the high dislocation density produced by SMAT or USP, the presence of residual  
622 stresses contributes also substantially to the improved yield strength and enhance strain hardening which  
623 helps to retain a good ductility. The effect of the processing parameters on the surface integrity and the  
624 importance of the subsurface residual stress relaxation on loading are highlighted for understanding the  
625 fatigue response of mechanical parts. Over Shot Peening (OSP) must be avoided.

626 In general, strengthening through grain refinement by SSPD does not sacrifice the corrosion  
627 resistance (Section 5.1). On the contrary, if properly located on the  $E_h$ -pH Pourbaix diagram, the

628 presence of structural defects modifies the surface reactivity and ease the formation of a passive film.  
629 However, as the peening treatments are based on impacts with the surface, inclusions from the  
630 processing media or local contaminations by abrasion of the treatment chamber are also important  
631 factors that can create local galvanic cells and encourage corrosion by pitting.

632 Due to the imparted severe plastic deformation and the high quantity of generated structural  
633 defects which enhance the surface reactivity, SMAT has been used within "duplex" treatments to assist  
634 the kinetics of diffusion for several thermochemical industrial processes such as nitriding, aluminizing,  
635 plasma electrolytic oxidation... Here again, the presence of surface contamination can be an issue  
636 (Section 5.2).

637 The recent results reviewed in section 5.4 show that having a rough surface with improved  
638 "reactivity" towards human cells as generated a new active field of research for SSPD. Indeed,  
639 bio-medical applications now in development both towards biocompatible Ti-based alloys and  
640 biodegradable Mg-based alloys.

641 Finally, some new research studies using SSPD for potential applications in the hydrogen  
642 sector are reviewed (section 5.3). Both hydrogen solid-state storage via the easier formation of metal  
643 hydride after SSPD and the protection of mechanical infrastructures via improvement of hydrogen  
644 embrittlement are considered.

645 Overall, SSPD techniques are generally cost-effective and chemical-free mechanical  
646 modification routes that are bringing viable solutions to different material sciences issues.

647

648

## 649 **7. Acknowledgements**

650 The authors would like to thank the support of the French State through the program "Investment in the  
651 future" operated by the National Research Agency (ANR) and referenced by ANR-11- LABX-0008-01  
652 (Labex DAMAS).

653

654 **8 Glossary**

655	ABSP	Air Blast Shot Peening
656	CG	Coarse Grain
657	CRS	Compressive Residual Stress
658	CSP	Conventional Shot Peening
659	CT	Cryogenic Temperature
660	EBSD	Electron BackScattered Diffraction
661	FSP	Friction Stir Process
662	GND	Geometrically Necessary Dislocation
663	HAGB	High Angle Grain Boundary
664	HE	Hydrogen Embrittlement
665	HEBM	High Energy Ball Milling
666	HEDE	Hydrogen-Enhanced Decohesion
667	HELP	Hydrogen-Enhanced Localized Plasticity
668	HESIV	Hydrogen-Enhanced Strain-Induced Vacancy
669	HDI	Hetero-Deformation Induced
670	hFOB	Human Fetal Osteoblast
671	HIPT	Hydrogen-Induced Phase Transformation
672	HPT	High Pressure Torsion
673	LAGB	Low Angle Grain Boundary
674	LSP	Laser Shot Peening
675	MRSA	Methicillin-Resistant Staphylococcus Aureus
676	MSC	Mesenchymal Stem Cells
677	NC	NanoCrystalline
678	OSP	Over Shot Peening
679	RASP	Rotationally Accelerated Shot Peening
680	RT	Room Temperature
681	SMAT	Surface Mechanical Attrition Treatment
682	SMRT	Surface Mechanical Rolling Treatment
683	SNH	Surface Nanocrystallization and Hardening
684	SP	Shot Peening
685	SPD	Severe Plastic Deformation
686	SSP	Severe Shot Peening
687	SSPD	Surface Severe Plastic Deformation
688	TC	Tension-Compression
689	TRIP	TRansformation Induced Plasticity
690	TT	Tension-Tension
691	UFG	Ultra Fine Grain

692	USNM	Ultrasonic Surface Nanocrystallization Modification
693	USP	Ultrasonic Shot Peening
694	VP	Vibratory Peening
695		

696 **9. References**

- 697 [1] H. Gleiter, *Acta Mater.*, **48**, no. 1, (2000), pp. 1–29,
- 698 [2] R. Z. Valiev, R. K. Islamgaliev, and I. V. Alexandrov, *Prog. Mater. Sci.*, **45**, no. 2, (2000), pp.  
699 103–189,
- 700 [3] Y. T. Zhu, T. C. Lowe, and T. G. Langdon, *Scripta Mater.*, **51**, (2004), pp. 825–830,
- 701 [4] K. Edalati *et al.*, *Mater. Res. Lett.*, **10**, no. 4, (2022), pp. 163–256,
- 702 [5] P. P. Shukla, P. T. Swanson, and C. J. Page, *Proc. Inst. Mech. Eng. Part B J. Eng. Manuf.*,  
703 **228**, no. 5, (2014), pp. 639–652,
- 704 [6] K. Lu and J. Lu, *Mater. Sci. Eng. A*, **375–377**, (2004), pp. 38–45,
- 705 [7] J. L. Liu, M. Umemoto, Y. Todaka, and K. Tsuchiya, *J. Mater. Sci.*, **42**, no. 18, (2007), pp.  
706 7716–7720,
- 707 [8] B. N. Mordyuk and G. I. Prokopenko, *J. Sound Vib.*, **308**, no. 3–5, (2007), pp. 855–866,
- 708 [9] X. Wang, Y. S. Li, Q. Zhang, Y. H. Zhao, and Y. T. Zhu, *J. Mater. Sci. Technol.*, **33**, no. 7,  
709 (2017), pp. 758–761,
- 710 [10] M. Multigner, S. Ferreira-Barragáns, E. Frutos, M. Jaafar, J. Ibáñez, P. Marín, M. T.  
711 Pérez-Prado, G. González-Doncel, A. Asenjo, and J. L. González-Carrasco, *Surf. Coatings*  
712 *Technol.*, **205**, no. 7, (2010), pp. 1830–1837,
- 713 [11] T. Grosdidier and M. Novelli, *Mater. Trans.*, **60**, no. 7, (2019), pp. 1344–1355,
- 714 [12] E. Maleki, S. Bagherifard, O. Unal, M. Bandini, G. H. Farrahi, and M. Guagliano, *Sci. Rep.*,  
715 **11**, no. 1, (2021), pp. 1–13,
- 716 [13] S. Q. Deng, A. Godfrey, W. Liu, and N. Hansen, *Scripta Mater.*, **117**, (2016), pp. 41–45,
- 717 [14] D. Liu, D. Liu, X. Zhang, C. Liu, and N. Ao, *Mater. Sci. Eng. A*, **726**, no. March, (2018), pp.  
718 69–81,

- 719 [15] C. S. Montross, T. Wei, L. Ye, G. Clark, and Y. W. Mai, *Int. J. Fatigue*, **24**, no. 10, (2002), pp.  
720 1021–1036,
- 721 [16] C. Zhang, Y. Dong, and C. Ye, *Adv. Eng. Mater.*, **23**, no. 7, (2021), pp. 1–24,
- 722 [17] D. I. Proskurovsky, V. P. Rotshtein, G. E. Ozur, Y. F. Ivanov, and A. B. Markov, *Surf.*  
723 *Coatings Technol.*, **125**, no. 1–3, (2000), pp. 49–56,
- 724 [18] J. X. Zou, T. Grosdidier, B. Bolle, K. M. Zhang, and C. Dong, *Metall. Mater. Trans. A*, **38 A**,  
725 no. 9, (2007), pp. 2061–2071,
- 726 [19] A. D. Pogrebnjak, V. S. Ladysev, N. A. Pogrebnjak, A. D. Michaliov, V. T. Shablya, A. N.  
727 Valyaev, A. A. Valyaev, and V. B. Loboda, *Vacuum*, **58**, no. 1. pp. 45–52, 2000.
- 728 [20] V. Schulze, F. Bleicher, P. Groche, Y. B. Guo, and Y. S. Pyun, *CIRP Ann. - Manuf. Technol.*,  
729 **65**, no. 2, (2016), pp. 809–832,
- 730 [21] I. Altenberger, B. Scholtes, U. Martin, and H. Oettel, *Mater. Sci. Eng. A*, **264**, no. 1–2, (1999),  
731 pp. 1–16,
- 732 [22] H. W. Huang, Z. B. Wang, J. Lu, and K. Lu, *Acta Mater.*, **87**, (2015), pp. 150–160,
- 733 [23] A. Kishore, M. John, A. M. Ralls, S. A. Jose, U. B. Kuruveri, and P. L. Menezes,  
734 *Nanomaterials*, **12**, no. 9, (2022),
- 735 [24] M. Malaki and H. Ding, *Mater. Des.*, **87**, (2015), pp. 1072–1086,
- 736 [25] S. Bagheri and M. Guagliano, *Surf. Eng.*, **25**, no. 1, (2009), pp. 3–14,
- 737 [26] K. Zhan, C. H. Jiang, X. Y. Wu, and V. Ji, *Mater. Trans. JIM*, **53**, no. 5, (2012), pp.  
738 1002–1006.
- 739 [27] J. W. Tian, J. C. Villegas, W. Yuan, D. Fielden, L. Shaw, P. K. Liaw, and D. L. Klarstrom,  
740 *Mater. Sci. Eng. A*, **468–470**, (2007), pp. 164–170,
- 741 [28] H. Y. Miao, D. Demers, S. Larose, C. Perron, and M. Lévesque, *J. Mater. Process. Technol.*,

- 742           **210**, no. 15, (2010), pp. 2089–2102,
- 743 [29] P. Fu, K. Zhan, and C. Jiang, *Mater. Des.*, **51**, (2013), pp. 309–314,
- 744 [30] T. O. Olugbade and J. Lu, *Nano Mater. Sci.*, **2**, no. 1, (2020), pp. 3–31,
- 745 [31] J. Badreddine, E. Rouhaud, M. Micoulaut, and S. Remy, *Int. J. Mech. Sci.*, **82**, (2014), pp.  
746           179–190,
- 747 [32] T. Das, A. Erdogan, B. Kursuncu, E. Maleki, and O. Unal, *Surf. Coatings Technol.*, **403**,  
748           (2020), p. 126383,
- 749 [33] H. Miao, L. Canals, B. McGillivray, and M. Lévesque, *Internatiol Conf. Shot Peen.*, (2017),  
750           pp. 521–526.
- 751 [34] W. Pfeiffer and T. Frey, *J. Eur. Ceram. Soc.*, **26**, no. 13, (2006), pp. 2639–2645,
- 752 [35] A. Heinzlmeier, A. Guitton, M. Novelli, W. Yu, and T. Grosdidier, *J. Alloys Compd.*, **950**,  
753           (2022), p. 169946,
- 754 [36] A. M. O. Mohamed, Z. Farhat, A. Warkentin, and J. Gillis, *J. Mater. Process. Technol.*, **277**,  
755           no. September 2019, (2020), p. 116399,
- 756 [37] W. Siguerdidjane, F. Khameneifar, and F. P. Gosselin, *HardwareX*, **11**, (2022), p. e00263,
- 757 [38] D. Fabijanic, A. Taylor, K. D. Ralston, M. X. Zhang, and N. Birbilis, *Corrosion*, **69**, no. 6,  
758           (2013), pp. 527–535,
- 759 [39] L. Wen, Y. Wang, Y. Zhou, L. X. Guo, and J. H. Ouyang, *Mater. Chem. Phys.*, **126**, no. 1–2,  
760           (2011), pp. 301–309,
- 761 [40] Y. Samih, M. Novelli, T. Thiriet, B. Bolle, N. Allain, J. J. Fundenberger, G. Marcos, T.  
762           Czerwicz, and T. Grosdidier, *IOP Conf. Ser. Mater. Sci. Eng.*, **63**, no. 1, (2014),
- 763 [41] L. Waltz, D. Retraint, A. Roos, C. Garnier, and P. Olier, *Surf. Coatings Technol.*, **205**, no. 19,  
764           (2011), pp. 4608–4613,

- 765 [42] Y. Samih, B. Beausir, B. Bolle, and T. Grosdidier, *Mater. Charact.*, **83**, (2013), pp. 129–138,
- 766 [43] G. Proust, D. Retraint, M. Chemkhi, A. Roos, and C. Demangel, *Microsc. Microanal.*, **21**, no.
- 767 4, (2015), pp. 919–926,
- 768 [44] W. Liu, X. Jin, B. Zhang, D. Yun, and P. Chen, *Materials (Basel)*, **12**, no. 1, (2019),
- 769 [45] N. R. Tao, Z. B. Wang, W. P. Tong, M. L. Sui, J. Lu, and K. Lu, *Acta Mater.*, **50**, no. 18, (2002),
- 770 pp. 4603–4616,
- 771 [46] S. Allain, J. P. Chateau, O. Bouaziz, S. Migot, and N. Guelton, *Mater. Sci. Eng. A*, **387–389**,
- 772 (2004), pp. 158–162,
- 773 [47] H. W. Zhang, Z. K. Hei, G. Liu, J. Lu, and K. Lu, *Acta Mater.*, **51**, no. 7, (2003), pp.
- 774 1871–1881,
- 775 [48] N. R. Tao and K. Lu, *Scripta Mater.*, **60**, no. 12, (2009), pp. 1039–1043,
- 776 [49] M. Novelli, P. Bocher, and T. Grosdidier, *Mater. Charact.*, **139**, (2018), pp. 197–207,
- 777 [50] S. Bahl, B. T. Aleti, S. Suwas, and K. Chatterjee, *Philos. Mag.*, **98**, no. 23, (2018), pp.
- 778 2095–2119,
- 779 [51] X. Shi, Y. Li, X. Zeng, Y. Liu, B. Chen, J. Lu, and D. Li, *J. Mater. Sci. Technol.*, **35**, no. 7,
- 780 (2019), pp. 1473–1478,
- 781 [52] A. Y. Chen, H. H. Ruan, J. Wang, H. L. Chan, Q. Wang, Q. Li, and J. Lu, *Acta Mater.*, **59**, no.
- 782 9, (2011), pp. 3697–3709,
- 783 [53] H. L. Chan, H. H. Ruan, A. Y. Chen, and J. Lu, *Acta Mater.*, **58**, no. 15, (2010), pp.
- 784 5086–5096,
- 785 [54] T. Roland, D. Retraint, K. Lu, and J. Lu, *Mater. Sci. Eng. A*, **445–446**, (2007), pp. 281–288,
- 786 [55] Z. Pu, S. Yang, G. L. Song, O. W. Dillon, D. A. Puleo, and I. S. Jawahir, *Scripta Mater.*, **65**,
- 787 no. 6, (2011), pp. 520–523,

- 788 [56] W. Xu, X. C. Liu, X. Y. Li, and K. Lu, *Acta Mater.*, **182**, (2020), pp. 207–214,
- 789 [57] C. Ye, S. Suslov, D. Lin, Y. Liao, and G. J. Cheng, *J. Appl. Phys.*, **115**, no. 21, (2014),
- 790 [58] W. Luo, H. Gong, Q. Wang, J. Lu, and M. Yan, *Mater. Lett.*, **157**, (2015), pp. 315–317,
- 791 [59] M. Dehghan, R. Miresmaeili, M. Askari-Paykani, and H. R. Shahverdi, *Met. Mater. Int.*, **28**,
- 792 no. 5, (2022), pp. 1232–1245,
- 793 [60] M. Novelli, J. J. Fundenberger, P. Bocher, and T. Grosdidier, *Appl. Surf. Sci.*, **389**, (2016), pp.
- 794 1169–1174,
- 795 [61] K. A. Darling, M. A. Tschopp, A. J. Roberts, J. P. Ligda, and L. J. Kecskes, *Scripta Mater.*,
- 796 **69**, no. 6, (2013), pp. 461–464,
- 797 [62] Y. Shen, C. Wen, X. Yang, Y. Pang, L. Sun, J. Tao, Y. Gong, and X. Zhu, *J. Mater. Eng.*
- 798 *Perform.*, **24**, no. 12, (2015), pp. 5058–5064,
- 799 [63] B. Cai, X. Ma, J. Moering, H. Zhou, X. Yang, and X. Zhu, *Mater. Sci. Eng. A*, **626**, (2015), pp.
- 800 144–149,
- 801 [64] H. A. Murdoch, K. A. Darling, A. J. Roberts, and L. Kecskes, *Metals (Basel)*, **5**, no. 2, (2015),
- 802 pp. 976–985,
- 803 [65] M. Novelli, R. Chulist, W. Skrotzki, E. P. George, and T. Grosdidier, *Appl. Phys. Lett.*,
- 804 **119.20**, no. September, (2021), p. 201912,
- 805 [66] H. Wang, G. Song, and G. Tang, *Surf. Coatings Technol.*, **282**, (2015), pp. 149–154,
- 806 [67] A. Wick, V. Schulze, and O. Vöhringer, *Mater. Sci. Eng. A*, **293**, no. 1–2, (2000), pp. 191–197,
- 807 [68] Y. Huang, W. C. Liu, and J. Dong, *Mater. Sci. Technol.*, **30**, no. 12, (2014), pp. 1481–1487,
- 808 [69] C. Ye, Y. Liao, and G. J. Cheng, *Adv. Eng. Mater.*, **12**, no. 4, (2010), pp. 291–297,
- 809 [70] A. Wick, V. Schulze, and O. Vöhringer, *Steel Res.*, **8**, (2000), pp. 316–321.
- 810 [71] X. Pan, X. Wang, Z. Tian, W. He, X. Shi, P. Chen, and L. Zhou, *J. Alloys Compd.*, **850**, (2021),

- 811 p. 156672,
- 812 [72] S. Kikuchi, I. Tanaka, S. Takesue, J. Komotori, and K. Matsumoto, *Surf. Coatings Technol.*,  
813 **344**, (2018), pp. 410–417,
- 814 [73] J. Liu, C. Ye, and Y. Dong, *Adv. Ind. Manuf. Eng.*, **2**, (2021), p. 100006,
- 815 [74] Tange, *SAE Trans.*, (1999), pp. 463–467.
- 816 [75] S. H. Lim, Z. Zhang, D. H. L. Seng, M. Lin, S. L. Teo, F. Wei, A. K. H. Cheong, S. Wang, and  
817 J. Pan, *J. Alloys Compd.*, **882**, (2021), p. 160701,
- 818 [76] J. Liu, S. Suslov, S. Li, H. Qin, Z. Ren, G. L. Doll, H. Cong, Y. Dong, and C. Ye, *Adv. Eng.*  
819 *Mater.*, **20**, no. 1, (2018), pp. 1–6,
- 820 [77] A. Amanov and Y. S. Pyun, *Surf. Coatings Technol.*, **326**, (2017), pp. 343–354,
- 821 [78] P. Wei, P. Hua, M. Xia, K. Yan, H. Lin, S. Yi, J. Lu, F. Ren, and Q. Sun, *Acta Mater.*, **240**,  
822 (2022), p. 118269,
- 823 [79] M. Kong, T. Zang, Z. Wang, L. Zhu, H. Zheng, S. Gao, and H. M. Ngwangwa, *J. Mater. Res.*  
824 *Technol.*, **23**, (2023), pp. 1947–1967,
- 825 [80] X. Yang, H. Pan, J. Zhang, H. Gao, B. Shu, Y. Gong, and X. Zhu, *Mater. Trans.*, **60**, no. 8,  
826 (2019), pp. 1543–1552,
- 827 [81] Y. Sun, *Tribol. Int.*, **57**, (2013), pp. 67–75,
- 828 [82] P. Maurel, L. Weiss, P. Bocher, E. Fleury, and T. Grosdidier, *Wear*, **430–431**, (2019), pp.  
829 245–255,
- 830 [83] X. H. Chen, J. Lu, L. Lu, and K. Lu, *Scripta Mater.*, **52**, no. 10, (2005), pp. 1039–1044,
- 831 [84] X. L. Wu, M. X. Yang, F. P. Yuan, L. Chen, and Y. T. Zhu, *Acta Mater.*, **112**, (2016), pp.  
832 337–346,
- 833 [85] L. Waltz, D. Retraint, A. Roos, and P. Olier, *Scripta Mater.*, **60**, no. 1, (2009), pp. 21–24,

- 834 [86] M. X. Yang, R. G. Li, P. Jiang, F. P. Yuan, Y. D. Wang, Y. T. Zhu, and X. L. Wu, *Mater. Res.*  
835 *Lett.*, **7**, no. 11, (2019), pp. 433–438,
- 836 [87] M. Yang, Y. Pan, F. Yuan, Y. Zhu, and X. Wu, *Mater. Res. Lett.*, **4**, no. 3, (2016), pp. 145–151,
- 837 [88] Y. Zhu, K. Ameyama, P. M. Anderson, I. J. Beyerlein, H. Gao, H. S. Kim, E. Lavernia, S.  
838 Mathaudhu, H. Mughrabi, R. O. Ritchie, N. Tsuji, X. Zhang, and X. Wu, *Mater. Res. Lett.*, **9**,  
839 no. 1, (2021), pp. 1–31,
- 840 [89] P. Gao, Z. Sun, and D. Restraint, *Metals (Basel)*, **12**, no. 5, (2022),
- 841 [90] R. Chen, H. Xue, and B. Li, *Metals (Basel)*, **12.4**, no. 4, (2022), p. 642.
- 842 [91] P. S. Maiya and D. E. Busch, *Metall. Trans. A*, **6**, (1975), pp. 1761–1766,
- 843 [92] G. A. Webster and A. N. Ezeilo, *Int. J. Fatigue*, **23**, (2001), pp. 375–383,
- 844 [93] K. Dai and L. Shaw, *Mater. Sci. Eng. A*, **463**, no. 1–2, (2007), pp. 46–53,
- 845 [94] I. F. Pariente and M. Guagliano, *Surf. Coat. Technol.*, **202**, (2013), pp. 3072–3080.
- 846 [95] J. Zhou, Z. Sun, P. Kanouté, and D. Restraint, *Int. J. Fatigue*, **103**, (2017), pp. 309–317,
- 847 [96] S. A. Kumar, S. G. S. Raman, and T. S. N. S. Narayanan, *Trans. Indian Inst. Met.*, **67**, no. 1,  
848 (2014), pp. 137–141,
- 849 [97] G. Chen, J. Gao, Y. Cui, H. Gao, X. Guo, and S. Wu, *J. Alloys Compd.*, **735**, (2018), pp.  
850 536–546,
- 851 [98] V. Pandey, K. Chattopadhyay, N. C. Santhi Srinivas, and V. Singh, *Int. J. Fatigue*, **103**,  
852 (2017), pp. 426–435,
- 853 [99] P. Maurel, L. Weiss, T. Grosdidier, and P. Bocher, *Int. J. Fatigue*, **140**, (2020), p. 105792,
- 854 [100] C. Dureau, M. Arzaghi, R. Massion, Y. Nadot, and T. Grosdidier, *Mater. Sci. Eng. A*, **840**,  
855 (2022), p. 142916,
- 856 [101] Q. Sun, Q. Han, X. Liu, W. Xu, and J. Li, *Surf. Coatings Technol.*, **328**, (2017), pp. 469–479,

- 857 [102] H. Miyamoto, *Mater. Trans. JIM*, **57**, no. 5, (2016).
- 858 [103] H. Miyamoto, M. Yuasa, M. Rifai, and H. Fujiwara, *Mater. Trans. JIM*, **60**, no. 7, (2019).
- 859 [104] K. D. Ralston and N. Birbilis, *Corrosion*, **66**, no. 7, (2010), pp. 0750051–07500513,
- 860 [105] L. Liu, Y. Li, and F. Wang, *J. Mater. Sci. Technol.*, **26**, no. 1, (2010), pp. 1–14,
- 861 [106] R. K. Gupta and N. Birbilis, *Corros. Sci.*, **92**, (2015), pp. 1–15,
- 862 [107] S. Bahl, S. R. K. Meka, S. Suwas, and K. Chatterjee, *ACS Biomater. Sci. Eng.*, **4**, no. 9,
- 863 (2018), pp. 3132–3142,
- 864 [108] T. Olugbade, C. Liu, and J. Lu, *Adv. Eng. Mater.*, **21**, no. 8, (2019), pp. 1–11,
- 865 [109] L. Wen, Y. Wang, Y. Jin, and X. Ren, *Corros. Eng. Sci. Technol.*, **50**, no. 6, (2015), pp.
- 866 425–432,
- 867 [110] Q. Sun, X. Liu, Q. Han, J. Li, R. Xu, and K. Zhao, *Surf. Coatings Technol.*, **337**, (2018), pp.
- 868 552–560,
- 869 [111] H. A. Murdoch, J. P. Labukas, A. J. Roberts, and K. A. Darling, *Jom*, **69**, no. 7, (2017), pp.
- 870 1170–1174,
- 871 [112] W. P. Tong, C. Z. Liu, W. Wang, N. R. Tao, Z. B. Wang, L. Zuo, and J. C. He, *Scripta Mater.*,
- 872 **57**, no. 6, (2007), pp. 533–536,
- 873 [113] T. Balusamy, T. S. N. Sankara Narayanan, and K. Ravichandran, *Surf. Coatings Technol.*,
- 874 **213**, (2012), pp. 221–228,
- 875 [114] X. Si, B. Lu, and Z. Wang, *J. Mater. Sci. Technol.*, **25**, no. 4, (2009), pp. 433–436.
- 876 [115] S. D. Lu, Z. B. Wang, and K. Lu, *Mater. Sci. Eng. A*, **527**, no. 4–5, (2010), pp. 995–1002,
- 877 [116] L. Wen, Y. Wang, Y. Zhou, L. Guo, and J. H. Ouyang, *Corros. Sci.*, **53**, no. 1, (2011), pp.
- 878 473–480,
- 879 [117] W. P. Tong, C. S. He, J. C. He, L. Zuo, N. R. Tao, and Z. B. Wang, *Appl. Phys. Lett.*, **89**, no. 2,

- 880 (2006), pp. 1–4,
- 881 [118] F. Meng, G. Miyamoto, Y. Todaka, and T. Furuhashi, *Mater. Trans. JIM*, **63**, no. 6, (2022), pp.
- 882 864–871.
- 883 [119] T. Thiriet, T. Czerwicz, D. Hertz, G. Marcos, T. Toll-Duchanoy, S. Migot, B. Brugier, M.
- 884 Foucault, and T. Belmonte, *Defect Diffus. Forum*, **323–325**, (2012), pp. 471–476,
- 885 [120] A. M. Gatey, S. S. Hosmani, C. A. Figueroa, S. B. Arya, and R. P. Singh, *Surf. Coatings*
- 886 *Technol.*, **304**, (2016), pp. 413–424,
- 887 [121] M. Chemkhi, D. Reirant, A. Roos, and C. Demangel, *Surf. Coatings Technol.*, **325**, (2017),
- 888 pp. 454–461,
- 889 [122] B. Sakintuna, F. Lamari-Darkrim, and M. Hirscher, *Int. J. Hydrogen Energy*, **32**, no. 9,
- 890 (2007), pp. 1121–1140,
- 891 [123] V. A. Yartys *et al.*, *Int. J. Hydrogen Energy*, **44**, no. 15, (2019), pp. 7809–7859,
- 892 [124] K. Edalati, E. Akiba, W. J. Botta, Y. Estrin, R. Floriano, D. Fruchart, T. Grosdidier, Z.
- 893 Horita, J. Huot, H. W. Li, H. J. Lin, Á. Révész, and M. J. Zehetbauer, *J. Mater. Sci. Technol.*,
- 894 **146**, (2023), pp. 221–239,
- 895 [125] J. J. Reilly and R. H. Wiswall, *Inorg. Chem.*, **13**, no. 1, (1974), pp. 218–222,
- 896 [126] S. Miraglia, P. De Rango, S. Rivoirard, D. Fruchart, J. Charbonnier, and N. Skryabina,
- 897 *Journal of Alloys and Compounds*, **536**. pp. 1–6, 2012.
- 898 [127] K. Edalati, J. Matsuda, H. Iwaoka, S. Toh, E. Akiba, and Z. Horita, *Int. J. Hydrogen Energy*,
- 899 **38**, no. 11, (2013), pp. 4622–4627,
- 900 [128] H. Kim, K. Sakaki, H. Ogawa, Y. Nakamura, J. Nakamura, E. Akiba, A. Machida, T.
- 901 Watanuki, and T. Proffen, *J. Phys. Chem. C*, **117**, no. 50, (2013), pp. 26543–26550,
- 902 [129] K. Edalati, M. Novelli, S. Itano, H. W. Li, E. Akiba, Z. Horita, and T. Grosdidier, *J. Alloys*

- 903            *Compd.*, **737**, (2018), pp. 337–346,
- 904 [130] M. Novelli, K. Edalati, S. Itano, H. W. Li, E. Akiba, Z. Horita, and T. Grosdidier, *Int. J.*  
905            *Hydrogen Energy*, **45**, no. 8, (2020), pp. 5326–5336,
- 906 [131] X. Li, X. Ma, J. Zhang, E. Akiyama, Y. Wang, and X. Song, *Acta Metall. Sin.*, **33**, no. 6,  
907            (2020), pp. 759–773,
- 908 [132] N. E. Laadel, M. El Mansori, N. Kang, S. Marlin, and Y. Boussant-Roux, *Int. J. Hydrogen*  
909            *Energy*, **47**, no. 76, (2022), pp. 32707–32731,
- 910 [133] T. An, S. Li, J. Qu, J. Shi, S. Zhang, L. Chen, S. Zheng, and F. Yang, *Int. J. Fatigue*, **129**,  
911            (2019), p. 105235,
- 912 [134] K. Makoto, U. Wataru, and Y. Satoshi, *ISIJ Int.*, **61**, no. 4, (2021), pp. 1159–1169,
- 913 [135] Y. Wang, H. Xie, Z. Zhou, X. Li, W. Wu, and J. Gong, *Int. J. Hydrogen Energy*, **45**, no. 11,  
914            (2020), pp. 7169–7184,
- 915 [136] J. G. Kim, H. J. Seo, J. M. Park, S. M. Baek, A. Amanov, C. S. Lee, and H. S. Kim,  
916            *Materialia*, **9**, (2020), p. 100626,
- 917 [137] M. Safyari and M. Moshtaghi, *Hydrogen*, **2**, no. 3, (2021), pp. 377–385,
- 918 [138] A. Mohammadi, M. Novelli, M. Arita, J. W. Bae, H. S. Kim, T. Grosdidier, and K. Edalati,  
919            *Corros. Sci.*, **200**, (2022), p. 110253,
- 920 [139] M. Kaur and K. Singh, *Mater. Sci. Eng. C*, **102**, (2019), pp. 844–862,
- 921 [140] R. K. Agrawal, V. Pandey, A. Barhanpurkar-Naik, M. R. Wani, K. Chattopadhyay, and V.  
922            Singh, *Ultrasonics*, **104**, (2020), p. 106110,
- 923 [141] X. Luo, C. Liang, N. Li, Y. Zhu, N. Cao, J. Wang, K. Liu, H. Zhao, Z. Wang, and W. Wang, *J.*  
924            *Nanomater.*, **2020**, (2020), pp. 1–11,
- 925 [142] L. Weiss, Y. Nessler, M. Novelli, P. Laheurte, and T. Grosdidier, *Metals (Basel)*, **9**, no. 12,

- 926 (2019),
- 927 [143] P. Maurel, L. Weiss, P. Bocher, and T. Grosdidier, *Mater. Sci. Eng. A*, **803**, (2020), p. 140618.
- 928 [144] R. Huang, Y. Hao, Y. Pan, C. Pan, X. Tang, L. Huang, C. Du, R. Yue, and D. Cui, *RSC Adv.*,  
929 **12**, no. 31, (2022), pp. 20037–20053,
- 930 [145] J. Vishnu, A. R. Ansheed, P. Hameed, K. Praveenkumar, S. Pilz, L. Andrea Alberta, S.  
931 Swaroop, M. Calin, A. Gebert, and G. Manivasagam, *Appl. Surf. Sci.*, **586**, (2022), p. 152816,
- 932 [146] R. Zhang, S. Mankoci, N. Walters, H. Gao, H. Zhang, X. Hou, H. Qin, Z. Ren, X. Zhou, G. L.  
933 Doll, A. Martini, N. Sahai, Y. Dong, and C. Ye, *J. Biomed. Mater. Res. - Part B Appl.*  
934 *Biomater.*, **107**, no. 6, (2019), pp. 1854–1863,
- 935 [147] X. Shen, P. Shukla, P. Swanson, Z. An, S. Prabhakaran, D. Waugh, X. Nie, C. Mee, S.  
936 Nakhodchi, and J. Lawrence, *J. Alloys Compd.*, **801**, (2019), pp. 327–342,
- 937 [148] Y. Yang, Y. Lu, W. Shi, B. Hou, H. Qiao, J. Qi, E. Zhang, and G. Qin, *Opt. Laser Technol.*,  
938 **158**, (2023), p. 108794,
- 939 [149] C. Vasu, B. Venkateswarlu, R. V. Rao, B. Chanti, M. Saikrishna, and B. R. Sunil, *Mater.*  
940 *Today Proc.*, **15**, (2019), pp. 50–56,
- 941 [150] V. Badisha, S. Shaik, R. Dumpala, and B. R. Sunil, *Int. J. Miner. Metall. Mater.*, **27**, no. 7,  
942 (2020), pp. 962–969,
- 943 [151] V. K. Manivasagam, M. Sankar, C. B. Garcia, J. Vishnu, K. Chatterjee, S. Suwas, G.  
944 Manivasagam, and T. J. Webster, *Vitr. Model.*, **1**, no. 3, (2022), pp. 273–288,
- 945 [152] D. Singh, D. A. Basha, L. Wadsö, D. Orlov, Y. Matsushita, A. Singh, and S. S. Hosmani, *J.*  
946 *Alloys Compd.*, **882**, (2021), p. 160659,
- 947
- 948

949 **10. List of captions**

950 **Figure 1** Schematic representations of different mechanical surface treatments: a)  
951 deep-rolling or SMRT, b) hammering or USNM, c) RASP, d) ABSP, e) SMAT, f) USP and g) VP.  
952

953 **Figure 2** a) Representation of a gradient produced by SSPD (from [11]) and b) Thickness  
954 evolution of the different layers depending of the SMAT conditions for the 316L stainless steel  
955 (from [42]).  
956

957 **Figure 3** Effect of the ultrasonic SMAT temperature on the cross-section hardness gradient  
958 (RT = 20 °C, CT = -130 °C). Dotted lines represent the hardness measured after SMAT under  
959 CT [60].  
960

961 **Figure 4** Cross-section hardness of a 304 stainless steel treated by electropulsing-assisted  
962 ultrasonic surface rolling process for different temperatures ranging from 25 to 180 °C (higher  
963 current corresponds to higher temperature) [66]  
964

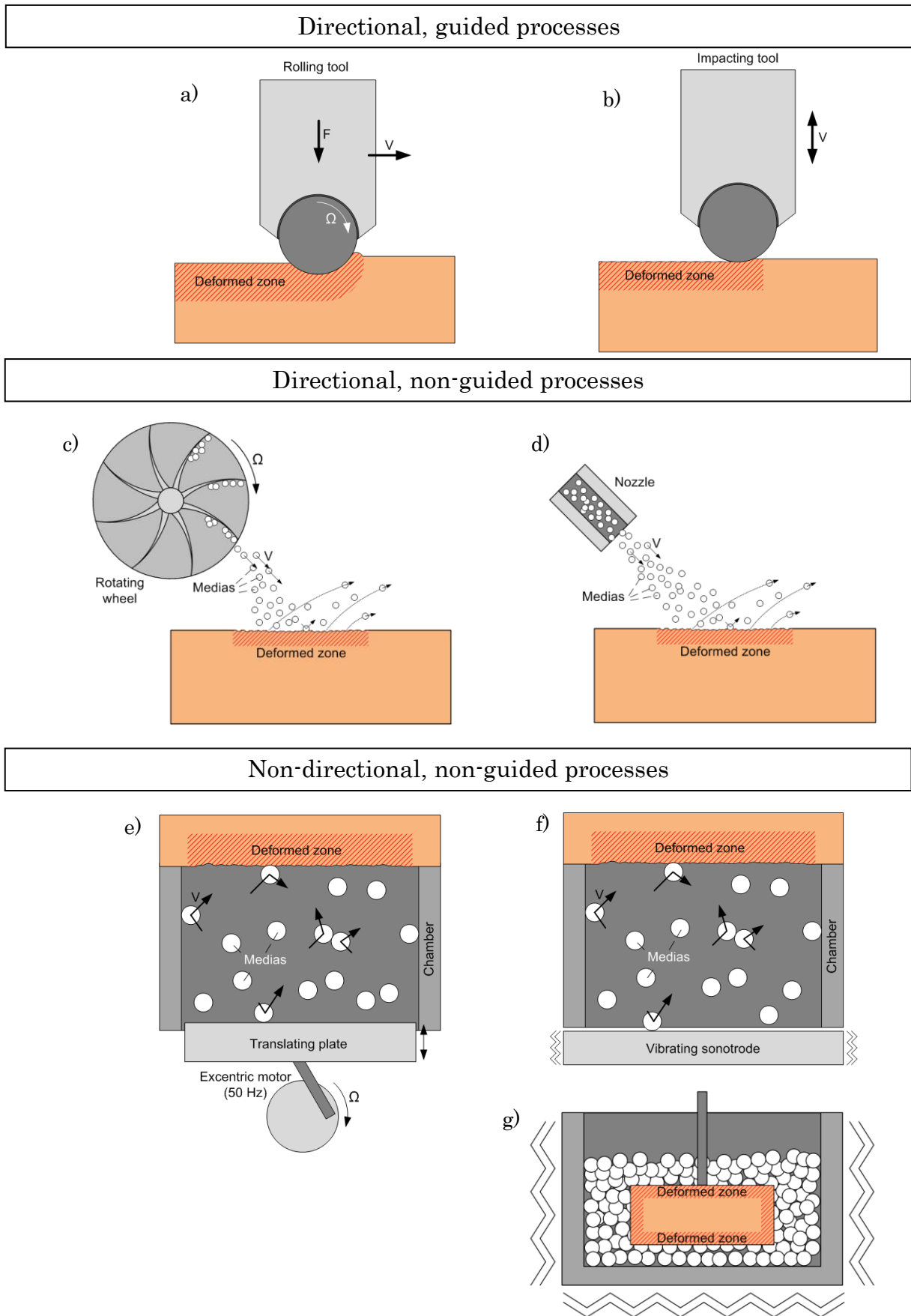
965 **Figure 5** Effect of the SMAT temperature on the surface hardness as a function of the surface  
966 roughness  $R_q$  of the 304L (flat samples) and 316L (round samples) stainless steels. Numbers  
967 closed to markers correspond to the treatment temperatures given in Celsius degrees (from  
968 -130°C to 500 °C). Adapted from [49].  
969

970 **Figure 6** Representation of a gradient produced by mechanical surface treatment and the  
971 corresponding mechanics on chemical diffusion and hydrogen absorption [130].  
972

973 **Figure 7** Representation of the HE-resistance mechanism developed in a SP layer [133].  
974

975 **Figure 8** Effect of polishing, SMAT and SMAT+polishing on cells adhesion (human  
976 mesenchymal stem cells) and subsequent proliferation along the FGM for different amount of  
977 Nb or Mo. (a) 0%; (b) 25%; (c) 50%; (d) 75%; (e) 100% from Weiss *et al.* [142]  
978

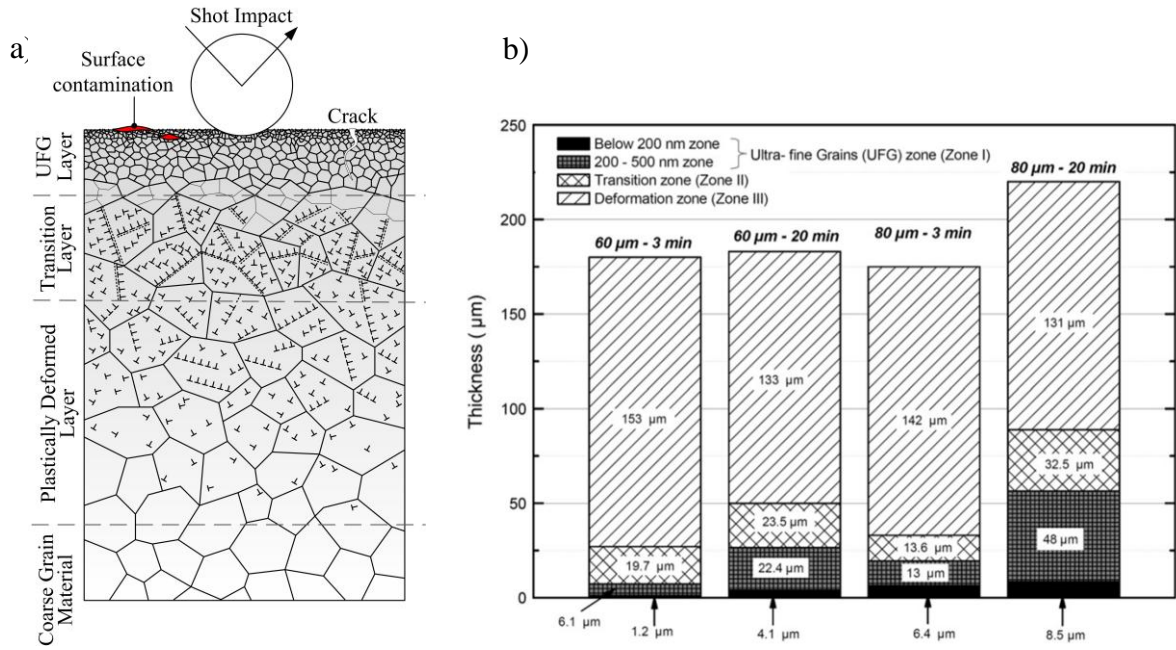
979 **Figure 9** Typical *Staphylococcus aureus* colonies after 24 h incubation on (a) CP Ti, (b) Ti-3Cu  
980 before LSP, Ti-3Cu after LSP (c) 5J-3, and (d)7J-3, (e) antibacterial rate of alloys against *S.*  
981 *aureus* relative to CP Ti. From Yang *et al.* [148].  
982



983

984 **Figure 1** Schematic representations of different mechanical surface treatments: a)

985 deep-rolling or SMRT, b) hammering or USNM, c) RASP, d) ABSP, e) SMAT, f) USP and g) VP.

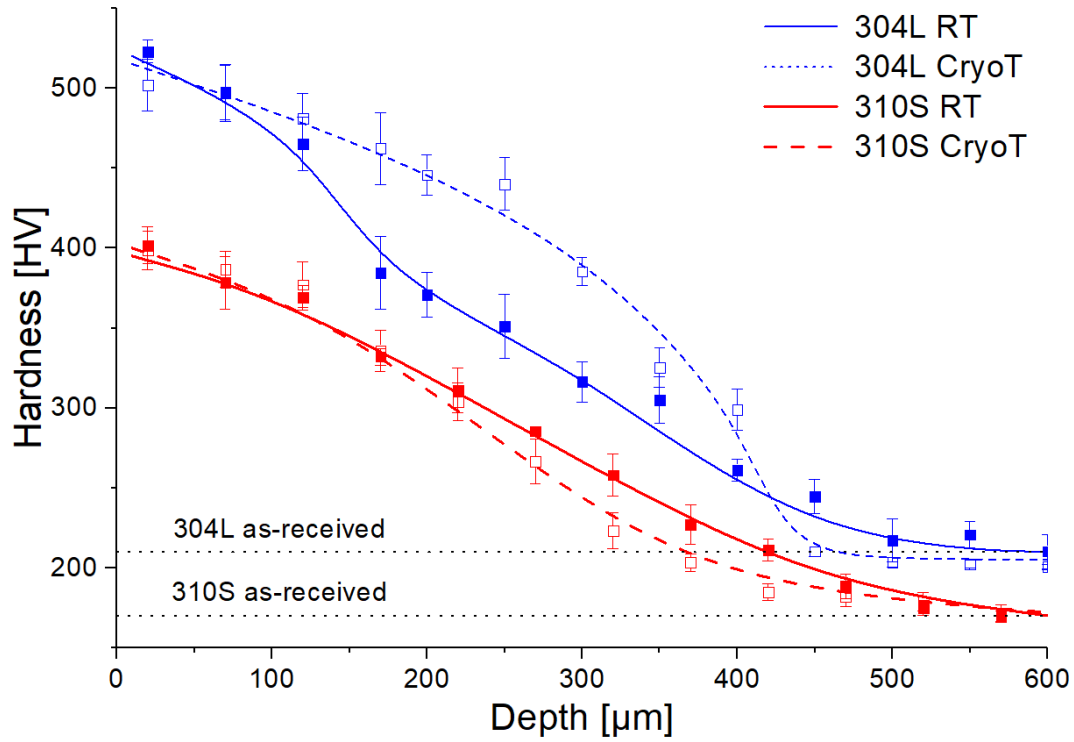


986

987

988 **Figure 2** a) Representation of a gradient produced by SSPD (from [11]) and b) Thickness  
 989 evolution of the different layers depending of the SMAT conditions for the 316L stainless steel  
 990 (from [42]).

991

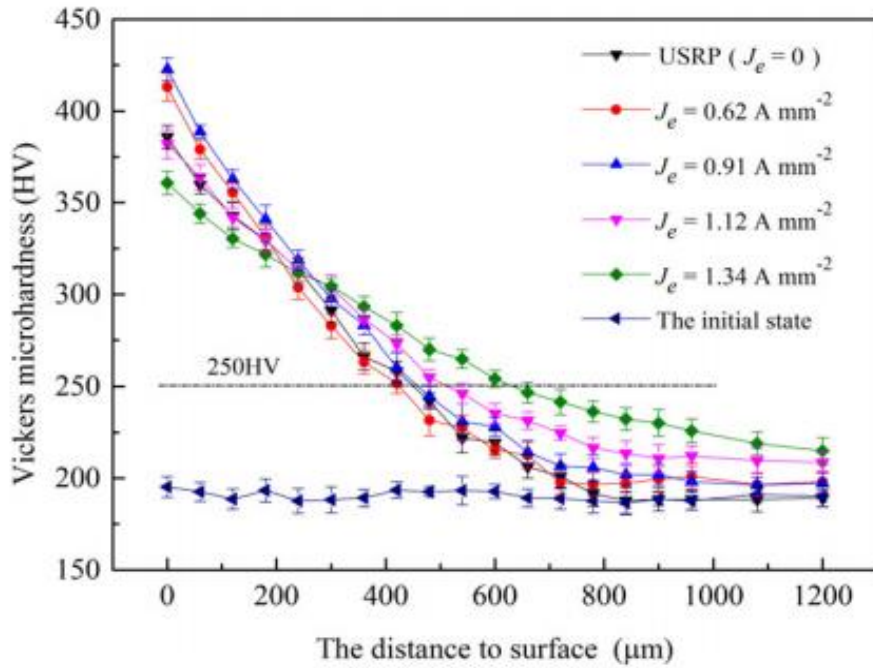


992

993

994 **Figure 3** Effect of the ultrasonic SMAT temperature on the cross-section hardness gradient  
 995 (RT = 20 °C, CT = -130 °C). Dotted lines represent the hardness measured after SMAT under  
 996 CT [60].

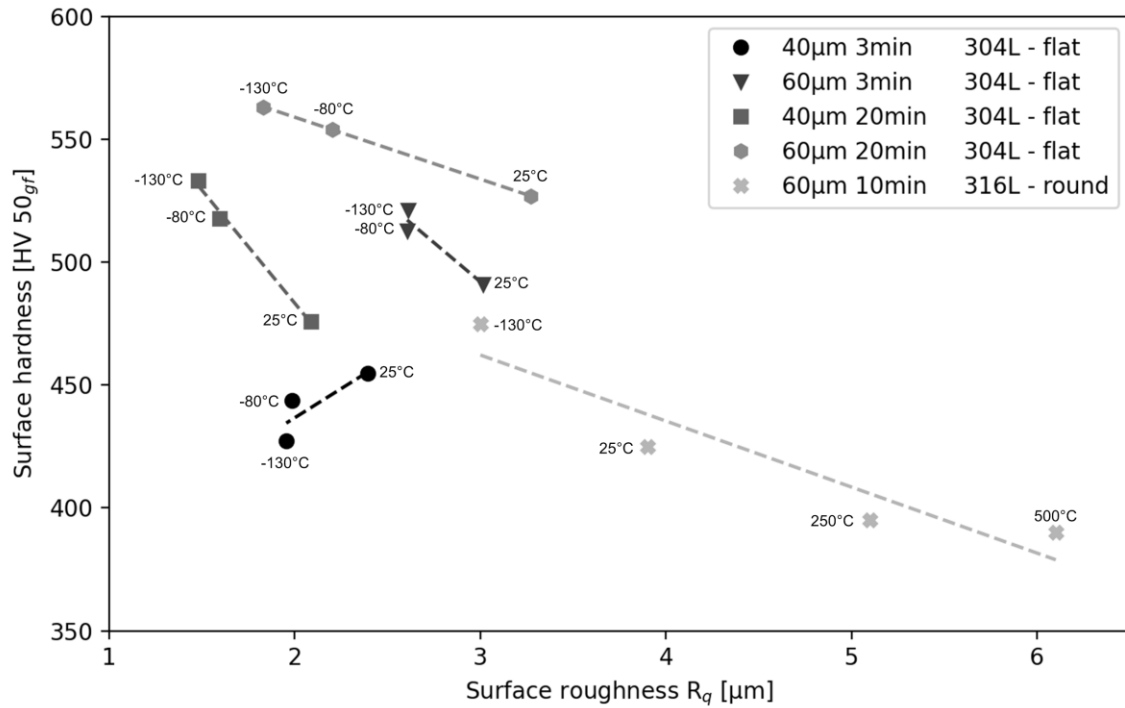
997



998

999

1000 **Figure 4** Cross-section hardness of a 304 stainless steel treated by electropulsing-assisted  
 1001 ultrasonic surface rolling process for different temperatures ranging from 25 to 180 °C (higher  
 1002 current corresponds to higher temperature) [66]  
 1003

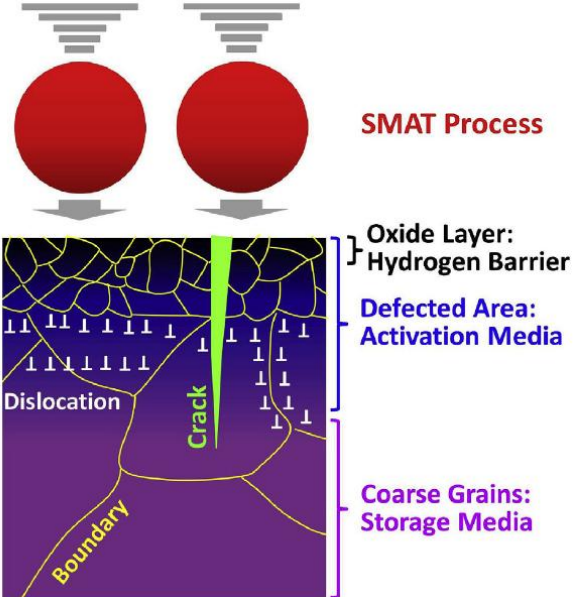


1004

1005

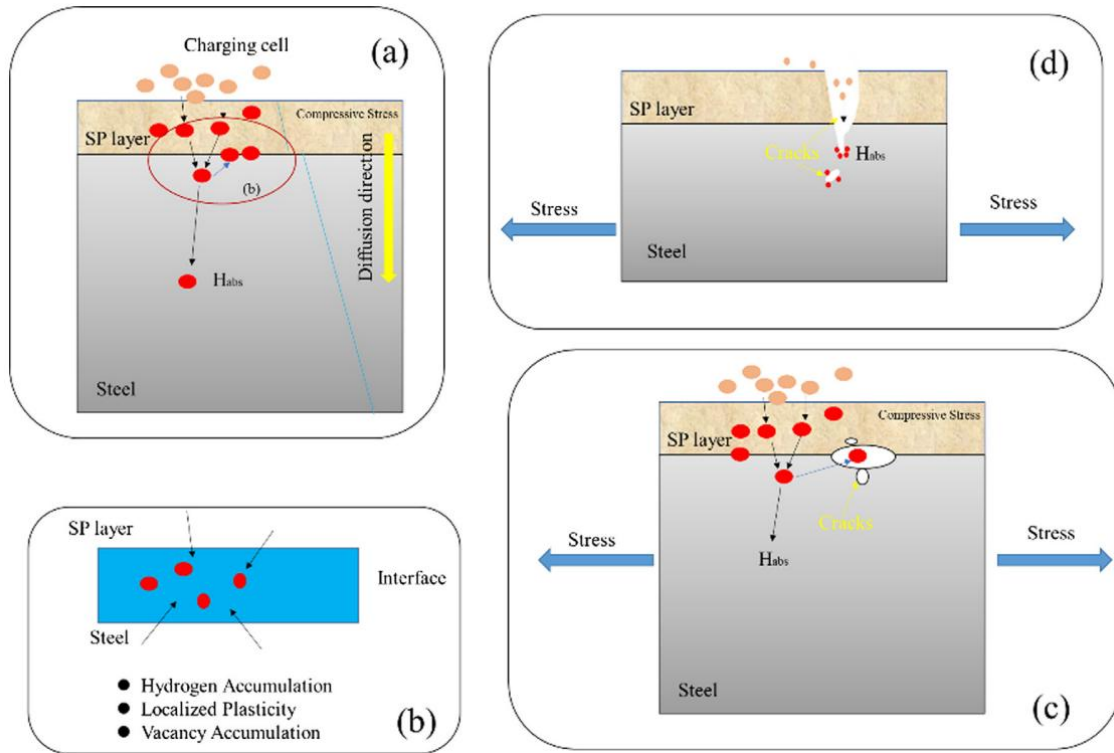
1006 **Figure 5** Effect of the SMAT temperature on the surface hardness as a function of the surface  
 1007 roughness  $R_q$  of the 304L (flat samples) and 316L (round samples) stainless steels. Numbers  
 1008 closed to markers correspond to the treatment temperatures given in Celsius degrees (from  
 1009 -130°C to 500 °C). Adapted from [49].

1010



1011  
1012  
1013  
1014  
1015

**Figure 6** Representation of a gradient produced by mechanical surface treatment and the corresponding mechanics on chemical diffusion and hydrogen absorption [129].

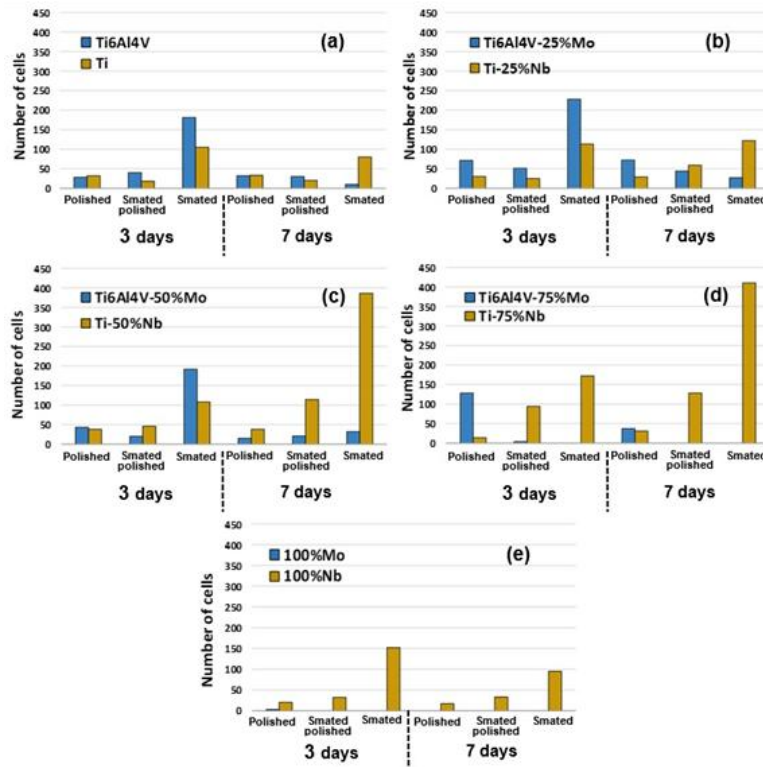


1016

1017

1018 **Figure 7** Representation of the HE-resistance mechanism developed in a SP layer [133].

1019

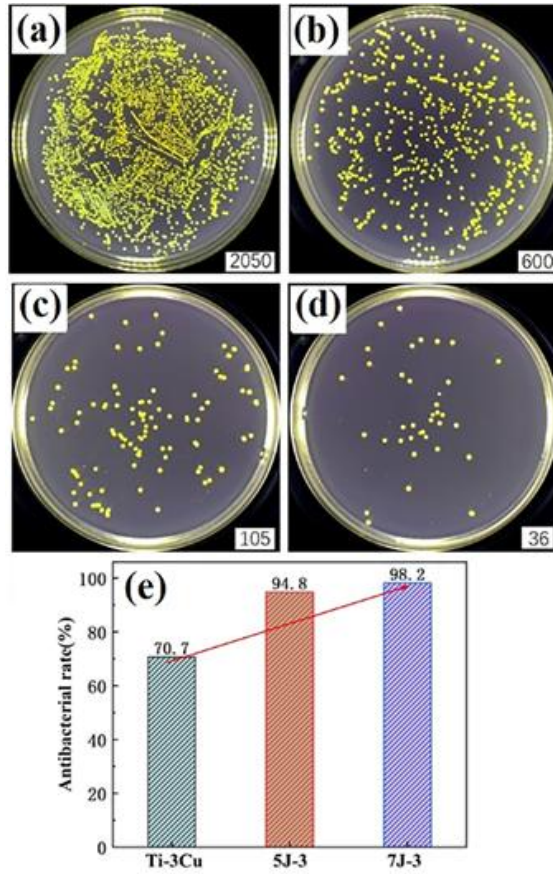


1020

1021

1022 **Figure 8** Effect of polishing, SMAT and SMAT+polishing on cells adhesion (human  
 1023 mesenchymal stem cells) and subsequent proliferation along the FGM for different amount of  
 1024 Nb or Mo. (a) 0%; (b) 25%; (c) 50%; (d) 75%; (e) 100% [142]

1025



1026

1027

1028 **Figure 9** Typical *Staphylococcus aureus* colonies after 24 h incubation on (a) CP Ti, (b) Ti-3Cu  
1029 before LSP, Ti-3Cu after LSP (c) 5J-3, and (d) 7J-3, (e) antibacterial rate of alloys against *S.*  
1030 *aureus* relative to CP Ti [148].

1031